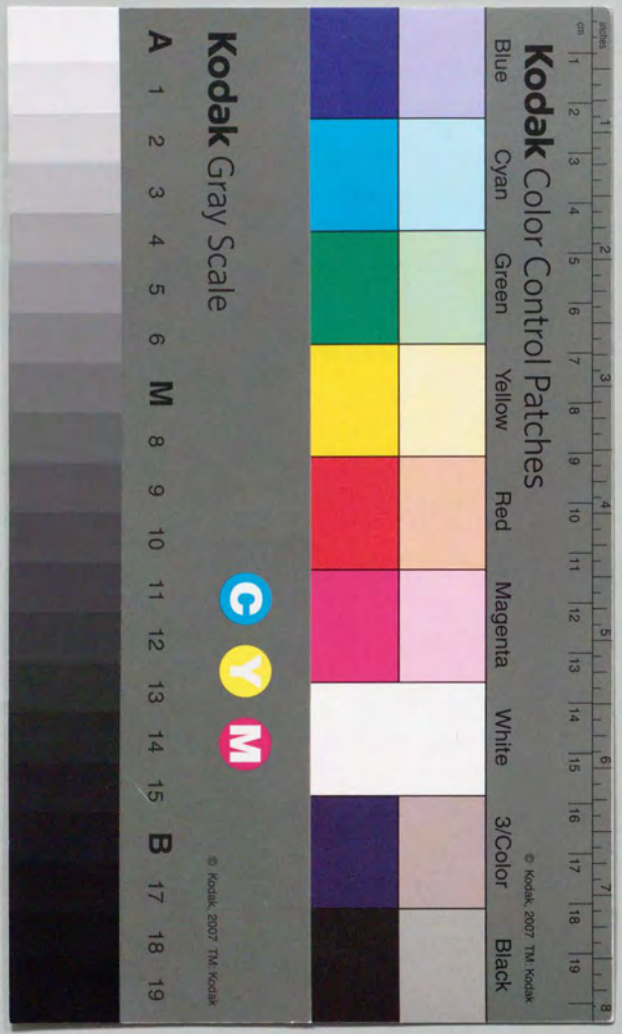

Thesis

学位論文

Measurement of laser pulse by intensity interference

強度干渉による レーザーパルスの測定

Submitted December, 1994

平成６年１２月博士（理学）申請

Department of Physics, Faculty of Science
University of Tokyo
東京大学大学院理学系研究科物理学専攻

Yoko Miyamoto
宮本洋子

①

Thesis

学位論文

Measurement of laser pulse by intensity interference

強度干渉による レーザーパルスの測定

Submitted December, 1994

平成６年１２月博士（理学）申請

Department of Physics, Faculty of Science
University of Tokyo
東京大学大学院理学系研究科物理学専攻

Yoko Miyamoto
宮本洋子

Contents

List of Figures

List of Tables

Chapter 1

Introduction

The study of intensity interference began with the work of Hanbury Brown and Twiss in 1956 [1] [2] [3] [4]. They were the first to observe interference effects in quantities that are fourth-order in terms of the amplitude of the optical field, as opposed to second-order interference effects such as was observed by Young [5] [6]. In their experiment, a beam of light from a mercury lamp was divided by a half-silvered mirror into two beams, whose intensity was measured by two photomultiplier tubes. It was shown that the fluctuations in the output currents of the two photodetectors are correlated when their cathode apertures as viewed from the source are superimposed, *i. e.* when the optical fields incident on the two cathodes are coherent with each other.

This correlation can be interpreted as a reflection of the correlation between the intensities of the two beams, or the correlation between the arrival times of photons at the two detectors. Before this it had been doubted that such a correlation could exist between two "coherent" beams of light. Indeed, no such correlation exists for the case of the classical stable wave [6], which has a fixed amplitude and phase, and is an example of "coherent" light. The above experiment showed that thermal radiation, while behaving as a classical stable wave (*i. e.* as "coherent" light) in second-order interference effects between two points in space-time that are close to each other, can exhibit, in terms of fourth-order interference, correlations that are non-existent in a classical stable wave.

This opened up a whole new interest in higher-order correlations, which was later formalized and given a quantum mechanical treatment by Glauber [7] [8]. In his work, Glauber defined a series of n-th order correlation functions, which express the correlation of values of the field at $2n$ different points in space-time, and describe interference effects of the $2n$-th order. The concept of coherence, which had formerly been understood as an ability of the field to exhibit second-order interference, was redefined in terms of a series of conditions to be fulfilled by these correlation functions. By this new definition, thermal radiation is only first-order coherent, because only the first-order correlation function fulfills the condition for coherence. In contrast the classical stable wave is fully coherent, *i. e.* coherent in all orders. A search for a quantum mechanical expression for a state of the electromagnetic field which fulfills the condition of full coherence led to the conception of the coherent state of radiation [9].

Intensity interference can be measured as correlations between photocurrents as by Hanbury Brown and Twiss, or, at lower power levels, as the rate of coincidence counts between two photon-counting detectors [10] [11]. It has been shown that information such as spectral width and the state of polarization of light can be obtained from these

correlations [12]. In the case of thermal or "quasithermal" radiation [13] [14] obeying Gaussian statistics, detailed information of the spectral distribution can be obtained by resolving the distribution of the time-difference of photon arrivals at the two detectors *. By increasing the number of detectors, measurement of third- and higher-order correlations are also possible.

It is of note that generally, studies in the field of intensity or fourth-order interference have traditionally been concerned with either *fluctuations* in light intensities and photon numbers, or with interference effects between photons from two independent sources [17] [18]. *Systematic* variations of intensity such as the envelope function of pulsed light have not been dealt with.

In many cases, semiclassical theory where a quantum mechanical model for the photodetection system and a classical model for the electromagnetic field are used can provide a sufficient explanation of the experimental results, even when the photon-counting method is used [19]. Of course, when the observed correlation cannot be explained by classical electromagnetic theory, a quantum mechanical treatment of the optical field is in order [20] [21] [22] [23] [24] [25] [26] [27].

It has been pointed out that the finite response time of the detectors and the electronic circuitry (typically of the order of nanoseconds) can pose a limit on the time-scale of fluctuations that can be measured by coincidence counting experiments [28] [29] [30]. Observation of fast decaying correlations is restricted in two ways:

1. The temporal profile of correlations that decay faster than the detector response time cannot be resolved.

2. Because of this, the coincidence count is measured as a time-integral during the response time of the detectors. This integrated quantity contains a large contribution from the non-interference term. The statistical noise (due to the stochastic nature of the photoemission process) of this non-interference component can easily obscure the contribution from the interference term.

The success of Hanbury Brown and Twiss lies in that:

- The focus was on spatial coherence rather than temporal coherence, with the photodetector translated perpendicular to the beam rather than parallel.

*Alternatively, an equivalent measurement is possible with a single photodetector by measuring the rate of coincidence between the original detector signal and its delayed replica [13] [15] [16]. However, with this method a certain dead region in the delay time is inevitable, in order to eliminate coincidences between signals originating from the same photoelectron.

- The experiment was performed with photocurrents, with the optical field intensity much higher than the photon-counting level. This enabled them to reduce the relative contribution from the statistical noise within a short time.

Because of the above restrictions from the detector response time, second- and third-order correlations of fast pulses have been studied through nonlinear processes such as two photon fluorescence [31], second harmonic generation [32], and third harmonic generation [33]. These methods have played an important role in determining the nature of pulses generated by mode-locked lasers [34] [35] [36] [37] [38] [39] [40] [41], whose pulse widths were of the order of picoseconds and were too short to be measured directly.

In 1987, Hong, Ou, and Mandel showed that restriction 1 can be overcome by combining a Mach-Zehnder-interferometer-like configuration with the coincidence-counting technique [42]. Beams of signal and idler photons created by a parametric down-conversion process (constituting the two "arms" of the interferometer) are mixed by a beam splitter. Two photomultipliers are placed on either side of the beam splitter to detect the two output beams. It was found that the coincidence count rate between the two detectors falls to zero when the beam paths from the parametric crystal to the beam splitter for the signal and idler photons are of equal length, *i. e.* when a pair of signal and idler photons arrive simultaneously at the beam splitter. By measuring the coincidence count rate as a function of the beam splitter position, the temporal correlation between the signal and idler photons was resolved to orders of femtoseconds.

Another important aspect of this experiment is the appearance of a 100 % decrease or "dip" in the coincidence count rate. For classical experiments where the two "arms" of the interferometer are provided by dividing a beam of light with a beam splitter, the contribution from two photons passing through the same arm cannot be excluded. This limits the decrease in the coincidence count rate to 50 %. The 100 % decrease in the above experiment reflects the fact that there is only one photon in each "arm" of the interferometer, and thus is an intrinsically quantum mechanical effect [43] [44] [45] [46].

The success of Mandel's group led to a new series of coincidence counting experiments, where variations of the Mach-Zehnder-interferometer configuration were utilized in various ways to explore the quantum mechanical effects of radiation [47] [48] [49] [50] [51] [52] [53].

Experiments within the scope of classical theory were also performed, such as the observation of beat between two different frequencies of the continuous-wave (cw) argon laser [54] and the measurement of the coherence time of off-axis fluorescence from laser

dye [55]. However, these experiments were performed with cw sources, and no attempt has yet been made to apply this new technique to the measurement of pulses. Furthermore, a close analysis of the latter experiment shows that it is in fact equivalent to the measurement of the visibility curve of the second-order interference fringes created by the Mach-zehnder-interferometer configuration. In this experiment, two different types of fluctuations are present in the field intensities at the two detectors: the second-order interference fringes modulated by a "phase modulator" inserted in the interferometer, and the fluctuations of the original input field. Since the time resolution of "coincidence" is much faster than the modulation of the phase modulator but slow compared with the original intensity fluctuations, only the former contribution is observed. Thus, while successfully measuring the band width, this experiment is *not* a measurement of the intensity fluctuations in the input field.

The present work proposes a new scheme that measures both the coherence time and the pulse width of ultrafast laser pulses by coincidence counting. It is the first attempt to measure a systematic temporal variation of the intensity of light through intensity interference. While using effectively the same setup as that for the measurement of the coherence time of fluorescence above, it is capable of measuring the intensity fluctuation of the input field. It is from this new contribution to the coincidence count rate that the pulse envelope can be determined.

Chapter 2 gives a general theoretical treatment of the coincidence count rate of pulse trains, and presents the basic scheme for the interferometer. Theoretical results for the coincidence count rate dip are given for various types of laser pulses. Chapter 3 gives a summary of the experimental apparatus and the method for data analysis. Experimental results for pulses generated by the synchronously pumped Rhodamine 6G dye laser and the self-mode-locked titanium:sapphire laser are presented in chapter 4. The results are in good agreement with values obtained by the conventional second harmonic (SH) autocorrelation technique. Discussion of the theoretical and experimental results are given in chapter 5.

Chapter 2

Theory

In this chapter, a general treatment of intensity interference and coincidence count rates will be given. A scheme which employs a Michelson interferometer configuration and simultaneously measures the pulse width and coherence time of ultrafast laser pulses will be presented, and theoretical results for various types of laser pulses will be calculated.

2.1 General treatment

2.1.1 Intensity interference and coincidence count rate

Let us consider the case where we perform photon counting with two photodetectors D_1 and D_2. The electric field operators at time t at the two detectors are represented by $\hat{E}_1^{(\pm)}(t)$ and $\hat{E}_2^{(\pm)}(t)$, respectively, where $(\pm)$ is $(+)$ for the positive frequency component of the operator and $(-)$ for the negative frequency component. If we let η_1 and η_2 represent the quantum efficiencies of the two detectors, the photon count rates or the probabilities that a photon is detected by each detector for a state of the electromagnetic field $|\psi\rangle$ is given by

$$Rate_1 = \eta_1 \langle\psi|\hat{E}_1^{(-)}(t)\hat{E}_1^{(+)}(t)|\psi\rangle \tag{2.1}$$

$$Rate_2 = \eta_2 \langle\psi|\hat{E}_2^{(-)}(t)\hat{E}_2^{(+)}(t)|\psi\rangle. \tag{2.2}$$

Note that at the classical limit, the count rates are proportional to the intensity of the electric field at the respective detectors.

Now we calculate the coincidence count rate, or the probability that the two detectors each detect a photon simultaneously. This is given by

$$Rate_{12} = \eta_1\eta_2 \langle\psi|\hat{E}_1^{(-)}(t)\hat{E}_2^{(-)}(t)\hat{E}_2^{(+)}(t)\hat{E}_1^{(+)}(t)|\psi\rangle. \tag{2.3}$$

Again at the classical limit, this rate is proportional to the averaged product of the intensities at the two detectors.

If no correlation exists between the two intensities, $Rate_{12}$ simply becomes the product of $Rate_1$ and $Rate_2$. But if there is a correlation, it gives rise to a phenomenon known as intensity interference, so that

$$Rate_{12} = Rate_1 Rate_2 + \text{interference term}. \tag{2.4}$$

It has been shown that the photoemission process, including its stochastic nature, can be sufficiently described within the scope of semiclassical theory, *i. e.* with a quantum mechanical model for the photodetection system and a classical model for the electromagnetic field [19]. Therefore, unless the observed correlation is of an intrinsically quantum

mechanical nature, both the single-detector count rates and the coincidence count rate can be calculated using classical electromagnetic theory. For such a case, the probability that a "photon counting" detector issues a signal is proportional to the instantaneous classical intensity. We will assume the laser pulses treated in this work to fall within this criterion, and from now on limit our discussion to classical theory. We will also assume a linearly polarized optical field, which applies to most types of lasers.

2.1.2 Coincidence count rate for classical pulses

Let us first rewrite equation (2.3) for a classical scalar field:

$$Rate_{12} = \eta_1\eta_2 E_1^*(t)E_2^*(t)E_2(t)E_1(t). \tag{2.5}$$

In actual experiments, the count rate is measured as a time average during a finite measurement time τ_M. The responses of the photodetectors, too, are not instantaneous, but are defined by a finite response time. The concept of "coincidence" must also be redefined to account for the finite time resolution; any two signals that arrive within a certain resolution time τ_{CR} are considered "coincident". With the above considerations, the coincidence count rate becomes

$$\begin{aligned} Rate_{12} \;=\; & \frac{1}{\tau_M}\int_{\tau_0}^{\tau_0+\tau_M} dt \int_{-\tau_{CR}/2}^{\tau_{CR}/2} d\tau \int_{-\infty}^{\infty} dt_1 \int_{-\infty}^{\infty} dt_2 \\ & \eta_1(t-t_1)\eta_2(t+\tau-t_2)\langle E_1^*(t_1)E_2^*(t_2)E_2(t_2)E_1(t_1)\rangle. \end{aligned} \tag{2.6}$$

Angular brackets denote an average over a statistical ensemble. $\eta_1(t)$ and $\eta_2(t)$ are the response functions of the two detectors, each with a finite width τ_r, and satisfying

$$\eta_j = \int_{-\infty}^{\infty} dt\, \eta_j(t) \qquad (j = 1, 2). \tag{2.7}$$

When the light is a pulse train, and the relation

$$T_0 \gg \tau_r \gg \tau_p, \tau_* \tag{2.8}$$

exists between the pulse cycle T_0, detector response time τ_r as defined above, the pulse width τ_p, and the coherence time (or the inverse of the spectral width) τ_*, equation (2.6) can be made more simple. In such cases we can assume that $\langle E_1^*(t_1)E_2^*(t_2)E_2(t_2)E_1(t_1)\rangle$ has finite values only within short (width $\sim \tau_p$) intervals near $t_1 = n_1 T_0$ and $t_2 = n_2 T_0$, where n_1 and n_2 are integers. The functions $\eta_1(t-t_1)$ and $\eta_2(t+\tau-t_2)$ stay approximately constant within these intervals. Then

$$Rate_{12} \sim \frac{1}{\tau_M}\int_{\tau_0}^{\tau_0+\tau_M} dt \int_{-\tau_{CR}/2}^{\tau_{CR}/2} d\tau \sum_{n_1,n_2} \eta_1(t-n_1T_0)\eta_2(t+\tau-n_2T_0)I_{12}(n_1,n_2), \tag{2.9}$$

where

$$I_{12}(n_1,n_2) = \int_{(1\text{ pulse})} dt_1 \int_{(1\text{ pulse})} dt_2 \langle E_1^*(n_1T_0+t_1)E_2^*(n_2T_0+t_2)E_2(n_2T_0+t_2)E_1(n_1T_0+t_1)\rangle. \tag{2.10}$$

In the case of stationary pulse trains, $I_{12}(n_1,n_2)$ relies only on n_2-n_1 and can be written as $I_{12}(n_2-n_1)$. If measurements are performed under the condition

$$\tau_M \gg T_0 \gtrsim \tau_{CR}, \tag{2.11}$$

then only those terms satisfying $n_2-n_1=0$ contribute to the result. Assuming $\tau_M = NT_0$,

$$Rate_{12} \sim \frac{1}{\tau_M}\sum_{n_1}\int_{\tau_0}^{\tau_0+\tau_M} dt \int_{-\tau_{CR}/2}^{\tau_{CR}/2} d\tau \eta_1(t-n_1T_0)\eta_2(t+\tau-n_1T_0)I_{12}(0) \tag{2.12}$$

$$\sim \frac{1}{\tau_M} N \int_{-T_0/2}^{T_0/2} dt \int_{-\tau_{CR}/2}^{\tau_{CR}/2} d\tau \eta_1(t)\eta_2(t+\tau)I_{12}(0) \tag{2.13}$$

$$= \frac{N}{\tau_M}\eta_1\eta_2 I_{12}(0), \tag{2.14}$$

that is,

$$Rate_{12} \sim \eta_1\eta_2 \frac{I_{12}(0)}{T_0}. \tag{2.15}$$

Thus in order to obtain the coincidence count rate for stationary pulse trains, it is sufficient to calculate the quantity:

$$\frac{I_{12}(0)}{T_0} = \frac{1}{T_0}\int_{-T_0/2}^{T_0/2} dt_1 \int_{-T_0/2}^{T_0/2} dt_2 \langle E_1^*(t_1)E_2^*(t_2)E_2(t_2)E_1(t_1)\rangle. \tag{2.16}$$

2.2 Measurement scheme for laser pulse width

2.2.1 Interferometer

I now present a scheme for the simultaneous measurement of the pulse width and the coherence time of laser pulses. An interferometer plays a crucial role in this scheme.

Just what kind of information we can obtain from a coincidence count rate reading depends on what relationship we establish between the input optical field $E(t)$ and the field $E_1(t)$ and $E_2(t)$ at the two photodetectors. The interferometer introduces precisely this relationship. Previous works [42] [55] have shown that a Mach-Zehnder-interferometer-like configuration can be very effective. In this work, a variation of the Michelson interferometer has been chosen instead, mainly because it provides good beam overlap for a wide range of path differences.

Figure 2.1 shows the schematics of the interferometer employed in this work.

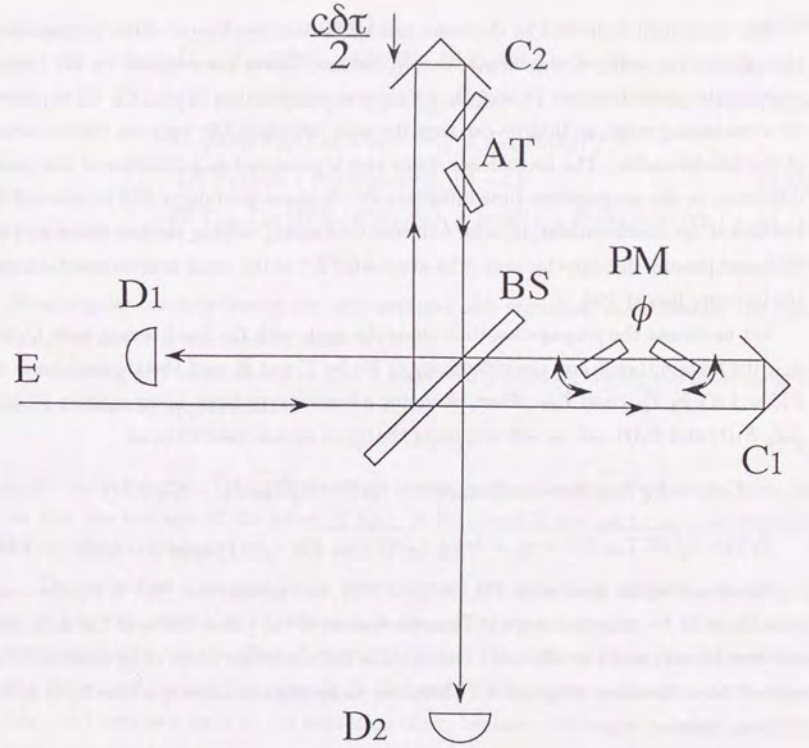

Figure 2.1: Measurement scheme:
E, input optical field; BS, beam splitter; D_1, D_2, photon-counting detectors; C_1, C_2, corner cubes; PM, phase modulator; AT, attenuator.

The input light is divided by the beam splitter BS into two beams. After propagating through the two arms of the interferometer, the two beams are remixed by BS before reaching the photodetectors D_1 and D_2. Of the two corner cubes C_1 and C_2, C_2 is placed on a translating stage, so that we can vary the path difference $c\,\delta\tau$ between the two arms of the interferometer. The coincidence count rate is measured as a function of this path difference, or the propagation time difference $\delta\tau$. A phase modulator PM is inserted in one arm of the interferometer, in order to introduce a slowly varying random phase $\phi(t)$ to the beam passing through this arm. The attenuator AT in the other arm counterbalances the intensity loss at PM.

Let us denote the propagation time along the path with the fixed corner cube C_1 by τ_{C1}, the transmittance and the reflectivity of BS by T and R, and the transmittance of PM and AT by T_{PM} and T_{AT}. Then, assuming a lossless symmetric beam splitter [5] [43] [44], $E_1(t)$ and $E_2(t)$ can be written, using the input optical field $E(t)$, as

$$E_1(t) = T\sqrt{T_{PM}}\,E(t-\tau_{C1})\,\exp[i\phi(t-\tau_{C1})] - R\sqrt{T_{AT}}\,E(t-\tau_{C1}+\delta\tau) \tag{2.17}$$

$$E_2(t) = i\sqrt{RT\,T_{AT}}\,E(t-\tau_{C1}+\delta\tau) + i\sqrt{RT\,T_{PM}}\,E(t-\tau_{C1})\,\exp[i\phi(t-\tau_{C1})]. \tag{2.18}$$

For simplicity let us redefine $E(t-\tau_{C1}) \to E(t)$, and assume that $E(t)$ is a pulse train with peaks at $t = nT_0$ (n: integer). Then the centers of the pulses arrive at the detectors at times $t = nT_0$ and $t = nT_0 + \delta\tau$. Realistically the maximum range of interest for $\delta\tau$ is several times the order of τ_p and τ_*. Therefore, under the condition specified by (2.8) we may assume that

$$T_0 \gg \tau_\tau \gg \delta\tau\,, \tag{2.19}$$

and the approximation made in (2.9) still holds for the above $E_1(t)$ and $E_2(t)$.

2.2.2 The role of the phase modulator

We now calculate the coincidence count rate for this interferometer, by substituting the formulas for $E_1(t)$ and $E_2(t)$ given in subsection 2.2.1 into equations (2.15) and (2.16):

$$\begin{aligned} Rate_{12}(\delta\tau) \quad &= \frac{\eta_1\eta_2}{T_0}\int_{-T_0/2}^{T_0/2}dt_1\int_{-T_0/2}^{T_0/2}dt_2 RT \\ &\left.\begin{array}{l}\langle T^2\,T_{PM}\,T_{AT}|E(t_1)|^2|E(t_2+\delta\tau)|^2 \\ +T^2\,T_{PM}^2|E(t_1)|^2|E(t_2)|^2 \\ +R^2\,T_{AT}^2|E(t_1+\delta\tau)|^2|E(t_2+\delta\tau)|^2 \\ +R^2\,T_{PM}\,T_{AT}|E(t_1+\delta\tau)|^2|E(t_2)|^2\end{array}\right\} \qquad (2.20a) \\ &-RT\,T_{PM}\,T_{AT}\{E^*(t_1)E^*(t_2+\delta\tau)E(t_1+\delta\tau)E(t_2)\exp[i\{\phi(t_2)-\phi(t_1)\}] \\ &\qquad +c.c.\} \qquad (2.20b) \\ &+\sqrt{T_{PM}\,T_{AT}}(T^2\,T_{PM}|E(t_1)|^2 + R^2\,T_{AT}|E(t_1+\delta\tau)|^2) \\ &\quad\cdot\{E^*(t_2+\delta\tau)E(t_2)\exp[i\phi(t_2)] + c.c.\} \qquad (2.20c) \\ &-RT\sqrt{T_{PM}\,T_{AT}}(T_{AT}|E(t_2+\delta\tau)|^2 + T_{PM}|E(t_2)|^2) \\ &\quad\cdot\{E^*(t_1)E(t_1+\delta\tau)\exp[-i\phi(t_1)] + c.c.\} \qquad (2.20d) \\ &-RT\,T_{PM}\,T_{AT}\{E^*(t_1)E^*(t_2)E(t_1+\delta\tau)E(t_2+\delta\tau)\exp[-i\{\phi(t_1)+\phi(t_2)\}] \\ &\qquad +c.c.\}\rangle. \qquad (2.20e) \end{aligned}$$

Here angular brackets denote not only averages over statistical ensembles for the input light, but also over the random phase $\phi(t)$.

Assuming $\phi(t)$ varies slowly so that it stays nearly constant during the pulse cycle T_0, we can make the approximation

$$\phi(t_1) = \phi(t_2) \tag{2.21}$$

in the above integral. Taking the average over $\phi(t)$ with this approximation in mind, we see that the averages of the terms (2.20c), (2.20d), and (2.20e) go to zero, so that only the contributions from (2.20a) and (2.20b) remain.

The terms that disappear in the above average are those that oscillate at frequencies ω_0 or $2\omega_0$ with respect to $\delta\tau$, where ω_0 is the carrier-wave frequency of $E(t)$. Thus the phase modulator has the effect of erasing these rapid oscillations in the coincidence count rate curve, and making the terms in (2.20a) and (2.20b) easier to observe. At the same time, $\phi(t)$ acts as a limit to the resolution of $\delta\tau$, because it averages out all fluctuations with respect to $\delta\tau$ that occur on a shorter time scale than the maximum range for $\phi(t)/\omega_0$. This also means that the path difference of the two arms of the interferometer need not be stable to an order shorter than the wavelength.

Under conditions (2.8) and (2.19), the intervals of integration for the four terms (2.20a) can be slightly altered to give a simplified expression for the coincidence count rate:

$$\begin{aligned} Rate_{12}(\delta\tau) \quad &= \frac{\eta_1\eta_2}{T_0}\cdot K_{IF}\int_{-T_0/2}^{T_0/2}dt_1\int_{-T_0/2}^{T_0/2}dt_2 \\ &\quad [\langle|E(t_1)|^2|E(t_2)|^2\rangle \\ &\quad -\frac{D_{IF}}{2}\{\langle E^*(t_1)E^*(t_2+\delta\tau)E(t_2)E(t_1+\delta\tau)\rangle + c.c.\}], \end{aligned} \tag{2.22}$$

where

$$K_{IF} = RT(T^2\,T_{PM} + R^2\,T_{AT})(T_{PM} + T_{AT}) \tag{2.23}$$

$$D_{IF} = \frac{2RT\,T_{PM}\,T_{AT}}{(T^2\,T_{PM} + R^2\,T_{AT})(T_{PM} + T_{AT})}\,. \tag{2.24}$$

Since we have assumed that $E(t)$ is nonzero only at $t \sim nT_0$, the contribution from the second term in the integrand exists only near $\delta\tau = 0$. Thus it can be seen that the coincidence count rate curve consists of a constant contribution from the first term and a decrease, or a 'dip' at $\delta\tau \sim 0$ from the second term. The relative depth of the dip at $\delta\tau = 0$ is determined by D_{IF}. D_{IF} depends solely on the parameters of the interferometer, and takes the maximum value 0.5 when the interferometer is perfectly balanced, *i. e.* $R = T = 1/2$ and $T_{PM} = T_{AT}$. The shape of the dip is determined by the characteristics of the ensemble average $\langle E^*(t_1)E^*(t_2+\delta\tau)E(t_2)E(t_1+\delta\tau)\rangle$.

We note in passing that behavior of a similar quantity has been studied for the case of integrated-intensity gratings [56] [57].

2.3 Coincidence count rate for various models

In order to obtain a more specific result, we need to make further assumptions about the input optical field $E(t)$. In the following will be discussed various models for laser pulse trains: models for perfect mode-locking, imperfect mode-locking, and two cases of chirped pulses. Results will be compared with those for the conventional second harmonic (SH) autocorrelation technique and the power spectra.

2.3.1 Perfectly mode-locked pulses

First let us consider pulse trains emitted by an ideally mode-locked laser, where the mode spacing and the relative phases of the modes are perfectly locked. For such a case we may write:

$$E(t) = \sum_k A_k \exp[-i(\omega_0 + k\Delta\omega_{ms})t], \tag{2.25}$$

where A_k is the fixed amplitude of the k-th mode and $\Delta\omega_{ms}$ is the mode separation.

Then $E(t)$ is a semiperiodic function where

$$E(t + 2\pi/\Delta\omega_{ms}) = E(t)\exp[-2\pi i\omega_0/\Delta\omega_{ms}] \tag{2.26}$$

so that

$$T_0 = 2\pi/\Delta\omega_{ms}. \tag{2.27}$$

Let us also note that this model has no statistical variable, so that no ensemble average is necessary with respect to $E(t)$.

For simplicity we choose A_k so that they are real and positive. It is not difficult to see that for such A_k, $|E(t)|$ has peaks with maximum value $\sum_k A_k$ at $t = nT_0$, in accordance

with our previous assumption. The width of the peaks are determined by $M\Delta\omega_{ms}$, where M is the number of modes that contribute to $E(t)$. After a time sufficiently longer than $2\pi/M\Delta\omega_{ms}$, contributions from different modes will have different phases so that $E(t) \sim 0$.

For our case of pulse trains that satisfy the condition (2.8), M can be considered very large. Then for a sufficiently smooth spectrum the sum in equation (2.25) can be approximated by an integral. For example, for a Gaussian spectrum

$$|A_k|^2 = K\exp[-(k\Delta\omega_{ms})^2/2\delta^2], \tag{2.28}$$

$E(t)$ is given by

$$\begin{aligned} E(t) &\sim \frac{1}{\Delta\omega_{ms}}\int d\omega\sqrt{K}\exp[-(\omega-\omega_0)^2/4\delta^2]\exp[-i(\omega-\omega_0)t]\exp(-i\omega_0 t) \\ &= \frac{2\delta\sqrt{\pi K}}{\Delta\omega_{ms}}\mathrm{e}^{-\delta^2t^2}\,\mathrm{e}^{-i\omega_0 t}. \end{aligned} \tag{2.29}$$

$E(t)$ given by equation (2.29) is no longer a periodic function, because by approximating the sum with an integral we have effectively taken T_0 to infinity. Here the pulse width $1/\delta$ is directly related to the inverse of the spectral width δ, so that there is no distinction between τ_p and τ_* in this model.

We now calculate the coincidence count rate for this $E(t)$. Substituting equation (2.29) in equation (2.22) we obtain:

$$Rate_{12}(\delta\tau) = \frac{\eta_1\eta_2}{T_0}\cdot K_{IF}{I_0}^2(1 - D_{IF}\,\mathrm{e}^{-\delta^2(\delta\tau)^2}), \tag{2.30}$$

where I_0 is the field intensity integrated over one pulse cycle and is given by

$$I_0 = \int_{-\infty}^{\infty} dt\left|\frac{2\delta\sqrt{\pi K}}{\Delta\omega_{ms}}\mathrm{e}^{-\delta^2t^2}\,\mathrm{e}^{-i\omega_0 t}\right|^2 = \frac{(2\pi)^{3/2}\delta K}{(\Delta\omega_{ms})^2}. \tag{2.31}$$

From equation (2.30) we see that the coincidence count rate is proportional to ${I_0}^2$. The shape of the dip is determined by the pulse shape, and the pulse width $1/\delta$ can be obtained by measuring the width of the dip.

For comparison let us calculate the autocorrelation curve obtained by the conventional SH autocorrelation technique. The average intensity of SH for the background-free configuration is given by:

$$I_{SH}(\delta\tau) = \frac{K_{SH}}{T_0}\int_{-T_0}^{T_0} dt\langle E^*(t)E^*(t+\delta\tau)E(t+\delta\tau)E(t)\rangle. \tag{2.32}$$

Here it has been assumed that the response of the SH crystal is instantaneous, *i. e.* that the response function $\chi(\tau)$ in the formula for the SH field:

$$E_{SH}(t;\delta\tau) = \int \delta\tau\, \chi(\tau) E(t-\tau) E(t+\delta\tau-\tau) \tag{2.33}$$

is a delta-function of τ. Substituting equation (2.29) we get:

$$I_{SH}(\delta\tau) = \frac{K_{SH}}{T_0} \cdot \frac{\delta}{\sqrt{\pi}}\, {I_0}^2 \mathrm{e}^{-\delta^2(\delta\tau)^2}. \tag{2.34}$$

Comparison with equation (2.30) shows that the dip closely resembles the SH autocorrelation curve.

2.3.2 Chaotic field

In subsection 2.3.1, the complex amplitudes A_k had been fixed, to reflect the nature of mode-locked pulses. Let us now consider the case where there is no mode locking, and the phases of A_k fluctuate independently. To reflect this fact we will assume a statistical ensemble for $\{A_k\}$ where the phases of A_k are independent random variables, and calculate various time-averaged quantities as an average $\langle\ \rangle_A$ over this ensemble.

Let us divide $E(t)$ in equation (2.25) into the carrier wave $\exp(-i\omega_0 t)$ and the random fluctuation $A(t)$ given by

$$A(t) = \sum_k A_k \exp(-i\, k\, \Delta\omega_{ms} t). \tag{2.35}$$

We now calculate the first-order correlation function of $A(t)$:

$$f(\tau) = \langle A^*(t)\, A(t+\tau)\rangle_A. \tag{2.36}$$

Substituting the definition for $A(t)$,

$$\begin{aligned} f(\tau) &= \langle \sum_k A_k^* \exp[+i\, k\, \Delta\omega_{ms}\, t] \sum_l A_l \exp[-i\, l\, \Delta\omega_{ms}(t+\tau)]\rangle_A \\ &= \sum_{k,l} \langle A_k^*\, A_l\rangle_A \exp[-i(l-k)\Delta\omega_{ms}\, t] \exp[-i\, l\, \Delta\omega_{ms}\, \tau]. \end{aligned} \tag{2.37}$$

Since the phases of different modes vary independently,

$$\langle A_k^*\, A_l\rangle_A = 0 \qquad (k \neq l). \tag{2.38}$$

Assuming a Gaussian spectrum:

$$\langle A_k^*\, A_k\rangle_A = K \exp[-(k\Delta\omega_{ms})^2/2\delta^2], \tag{2.39}$$

and again for large M approximating the sum with an integral as in equation (2.29), we obtain

$$\begin{aligned} f(\tau) &= \sum_k \langle A_k^*\, A_k\rangle_A \exp[-i\, k\, \Delta\omega_{ms}\, \tau] \\ &\sim \frac{1}{\Delta\omega_{ms}} \int d\omega K \exp[-(\omega-\omega_0)^2/2\delta^2] \exp[-i(\omega-\omega_0)\tau] \\ &= \frac{\sqrt{2\pi}\,\delta K}{\Delta\omega_{ms}} \mathrm{e}^{-\delta^2\tau^2/2}. \end{aligned} \tag{2.40}$$

Thus the coherence time, which can be defined as the width of $f(\tau)$, is given by $1/\delta$ and is equal to the inverse of the spectral width δ.

As we are interested in intensity interference, we also need to calculate the second-order correlation function:

$$\begin{aligned} \langle A^*(t_1)\, A^*(t_2)\, A(t_3)\, A(t_4)\rangle_A &= \langle \sum_{k_1} A_{k_1}^* \exp[+i\, k_1\, \Delta\omega_{ms}\, t_1] \sum_{k_2} A_{k_2}^* \exp[+i\, k_2\, \Delta\omega_{ms}\, t_2] \\ &\quad \sum_{k_3} A_{k_3} \exp[-i\, k_3\, \Delta\omega_{ms}\, t_3] \sum_{k_4} A_{k_4} \exp[-i\, k_4\, \Delta\omega_{ms}\, t_4]\rangle_A \\ &= \sum_{k_1,k_2,k_3,k_4} \langle A_{k_1}^*\, A_{k_2}^*\, A_{k_3}\, A_{k_4}\rangle_A \\ &\quad \exp[-i\Delta\omega_{ms}\,(k_3 t_3 + k_4 t_4 - k_1 t_1 - k_2 t_2)] \end{aligned} \tag{2.41}$$

The only non-zero contributions exist for

$$\begin{cases} k_1 = k_4 \\ k_2 = k_3 \end{cases} \qquad \text{and} \qquad \begin{cases} k_1 = k_3 \\ k_2 = k_4 \end{cases}, \tag{2.42}$$

so that

$$\begin{aligned} &\langle A^*(t_1)\, A^*(t_2)\, A(t_3)\, A(t_4)\rangle_A \\ &\quad = \sum_{k_1,k_2} \langle A_{k_1}^*\, A_{k_1}\rangle_A \langle A_{k_2}^*\, A_{k_2}\rangle_A \exp[-i\Delta\omega_{ms}\,\{k_1(t_4-t_1) + k_2(t_3-t_2)\}] \\ &\qquad + \sum_{k_1,k_2} \langle A_{k_1}^*\, A_{k_1}\rangle_A \langle A_{k_2}^*\, A_{k_2}\rangle_A \exp[-i\Delta\omega_{ms}\,\{k_1(t_3-t_1) + k_2(t_4-t_2)\}] \\ &\qquad - \sum_{k_1} \langle A_{k_1}^*\, A_{k_1}\rangle_A^2 \exp[-i\, k_1 \Delta\omega_{ms}\,(t_3 + t_4 - t_1 - t_2)]. \end{aligned} \tag{2.43}$$

The first two terms in equation (2.43) are of order M^2 while the third is of order M. Thus, for large M we obtain:

$$\begin{aligned} &\langle A^*(t_1)\, A^*(t_2)\, A(t_3)\, A(t_4)\rangle_A \\ &\quad \sim \sum_{k_1,k_2} \langle A_{k_1}^*\, A_{k_1}\rangle_A \langle A_{k_2}^*\, A_{k_2}\rangle_A \exp[-i\Delta\omega_{ms}\,\{k_1(t_4-t_1) + k_2(t_3-t_2)\}] \\ &\qquad + \sum_{k_1,k_2} \langle A_{k_1}^*\, A_{k_1}\rangle_A \langle A_{k_2}^*\, A_{k_2}\rangle_A \exp[-i\Delta\omega_{ms}\,\{k_1(t_3-t_1) + k_2(t_4-t_2)\}] \\ &\quad = \langle A^*(t_1)\, A(t_4)\rangle_A \langle A^*(t_2)\, A(t_3)\rangle_A + \langle A^*(t_1)\, A(t_3)\rangle_A \langle A^*(t_2)\, A(t_4)\rangle_A, \end{aligned} \tag{2.44}$$

or, in terms of $f(\tau)$,

$$\langle A^*(t_1)\, A^*(t_2)\, A(t_3)\, A(t_4)\rangle_A \sim f(t_4-t_1)f(t_3-t_2) + f(t_3-t_1)f(t_4-t_2). \qquad (2.45)$$

Similarly, higher-order correlation functions of $A(t)$ can be expressed as sums over various combinations of the first-order correlation function $f(\tau)$. This is a property known as Gaussian statistics, because the generating function of statistical variables that have this property has the form of a Gaussian function.

2.3.3 Imperfectly mode-locked pulses

$E(t)$ as defined in section 2.3.2 has no well-defined peak, and exhibits a random fluctuation whose time scale is specified by the coherence time $1/\delta$. To represent the imperfectly mode-locked laser where there is sufficient mode locking to create a well-defined pulse envelope but not enough to suppress all fluctuations, we introduce an envelope function $C(t)$ so that now we have [39]

$$E(t) = C(t)\, A(t)\, \exp(-i\omega_0 t). \qquad (2.46)$$

For simplicity we will assume a Gaussian spectrum for $A(t)$ as in subsection 2.3.2, and define K so that $f(0) = 1$, *i. e.*,

$$f(\tau) = \mathrm{e}^{-\delta^2\tau^2/2}. \qquad (2.47)$$

We will also assume a Gaussian shape for $C(t)$:

$$C(t) = C\,\mathrm{e}^{-t^2/{\tau_p}^2}. \qquad (2.48)$$

The spectral width of $E(t)$ is no longer given by δ because of the existence of $C(t)$. The power spectrum $G(\omega)$ can be calculated using the formula:

$$G(\omega) = \int_{-\infty}^{\infty} d\tau R(\tau)\exp(-i\omega\tau) + \text{c.c.} \quad , \qquad (2.49)$$

where

$$R(\tau) = \frac{1}{T_0}\int_{-T_0/2}^{T_0/2} dt \langle E^*(t+\tau)E(t)\rangle_A . \qquad (2.50)$$

Using equations (2.36), (2.46), (2.47), and (2.48),

$$\begin{aligned} R(\tau) &= \frac{1}{T_0}\int_{-T_0/2}^{T_0/2} dt C(t+\tau)C(t)f(-\tau)\exp(i\omega_0\tau) \\ &\sim \frac{1}{T_0}\int_{-\infty}^{\infty} dt C^2\,\mathrm{e}^{-[(t+\tau)^2+t^2]/{\tau_p}^2}\,\mathrm{e}^{-\delta^2\tau^2/2}\,\mathrm{e}^{i\omega_0\tau} \\ &= \frac{I_0}{T_0}\mathrm{e}^{-\tau^2/2{\tau_*}^2}\,\mathrm{e}^{i\omega_0\tau}, \end{aligned} \qquad (2.51)$$

where

$$I_0 = \int_{-\infty}^{\infty} dt C^2\,\mathrm{e}^{-2t^2/{\tau_p}^2} = \sqrt{\frac{\pi}{2}}\,C^2\tau_p \qquad (2.52)$$

and

$$\frac{1}{{\tau_*}^2} = \frac{1}{{\tau_p}^2} + \delta^2. \qquad (2.53)$$

Substituting into equation (2.49), we obtain:

$$G(\omega) = \frac{2\pi C^2\tau_p\tau_*}{T_0}\,\mathrm{e}^{-{\tau_*}^2(\omega-\omega_0)^2/2}. \qquad (2.54)$$

Thus the spectrum width is given by $1/\tau_*$ and the coherence time by τ_*. When τ_p is much longer than $1/\delta$, $\tau_* \sim 1/\delta$. As τ_p approaches $1/\delta$, the power spectrum is strongly modified by the existence of $C(t)$. The origin of $C(t)$ in this model is not clear in terms of the mode structure, so we should be careful in applying it to this regime.

Let us now calculate the coincidence count rate for this field. Substituting equation (2.46) into equation (2.22),

$$\begin{aligned} Rate_{12}(\delta\tau) &= \frac{\eta_1\eta_2}{T_0}\cdot K_{IF}\int_{-T_0/2}^{T_0/2} dt_1\int_{-T_0/2}^{T_0/2} dt_2 \\ &\quad [C^2(t_1)C^2(t_2)\langle |A(t_1)|^2|A(t_2)|^2\rangle_A \\ &\quad -\frac{D_{IF}}{2}C(t_1)C(t_2+\delta\tau)C(t_2)C(t_1+\delta\tau) \\ &\quad \cdot\{\langle A^*(t_1)\, A^*(t_2+\delta\tau)\, A(t_2)\, A(t_1+\delta\tau)\rangle_A + \text{c.c.}\}]. \end{aligned} \qquad (2.55)$$

Using equation (2.44) we get:

$$\begin{aligned} Rate_{12}(\delta\tau) &= \frac{\eta_1\eta_2}{T_0}\cdot K_{IF}\int_{-T_0/2}^{T_0/2} dt_1\int_{-T_0/2}^{T_0/2} dt_2 \\ &\quad [C^2(t_1)C^2(t_2) \\ &\quad \cdot\{\langle |A(t_1)|^2\rangle_A\langle |A(t_2)|^2\rangle_A + \langle A^*(t_1)\, A(t_2)\rangle_A\langle A^*(t_2)\, A(t_1)\rangle_A\} \\ &\quad -\frac{D_{IF}}{2}C(t_1)C(t_2+\delta\tau)C(t_2)C(t_1+\delta\tau) \\ &\quad \cdot\{(\langle A^*(t_1)\, A(t_1+\delta\tau)\rangle_A\langle A^*(t_2+\delta\tau)\, A(t_2)\rangle_A \\ &\quad +\langle A^*(t_1)\, A(t_2)\rangle_A\langle A^*(t_2+\delta\tau)\, A(t_1+\delta\tau)\rangle_A) + \text{c.c.}\}]. \end{aligned} \qquad (2.56)$$

Substituting equations (2.36), (2.47), and (2.48), we obtain:

$$\begin{aligned} &Rate_{12}(\delta\tau) \\ &= \frac{\eta_1\eta_2}{T_0}\cdot K_{IF}\int_{-T_0/2}^{T_0/2} dt_1\int_{-T_0/2}^{T_0/2} dt_2 \\ &[C^2(t_1)C^2(t_2)\{|f(0)|^2 + |f(t_2-t_1)|^2\} \end{aligned}$$

$$
\begin{aligned}
&-D_{IF}C(t_1)C(t_2+\delta\tau)C(t_2)C(t_1+\delta\tau)\{|f(\delta\tau)|^2+|f(t_2-t_1)|^2\}] \\
&\sim \frac{\eta_1\eta_2}{T_0}\cdot K_{IF}C^4\int_{-\infty}^{\infty}dt_1\int_{-\infty}^{\infty}dt_2 \\
&[\,\mathrm{e}^{2[{t_1}^2+{t_2}^2]/{\tau_p}^2}\{1+\mathrm{e}^{-\delta^2(t_2-t_1)^2}\} \\
&-D_{IF}\mathrm{e}^{-[{t_1}^2+(t_2+\delta\tau)^2+{t_2}^2+(t_1+\delta\tau)^2]/{\tau_p}^2}\{\mathrm{e}^{-\delta^2(\delta\tau)^2}+\mathrm{e}^{-\delta^2(t_2-t_1)^2}\}] \\
&=\frac{\eta_1\eta_2}{T_0}\cdot K_{IF}[{I_0}^2+I_1I_0-D_{IF}\{{I_0}^2\mathrm{e}^{-(\delta\tau)^2/{\tau_*}^2}+I_1I_0\mathrm{e}^{-(\delta\tau)^2/{\tau_p}^2}\}], \qquad (2.57)
\end{aligned}
$$

where

$$I_1=\int_{-\infty}^{\infty}dtC^2\mathrm{e}^{-2t^2/{\tau_*}^2}=\sqrt{\frac{\pi}{2}}C^2\tau_*. \qquad (2.58)$$

Since $I_1/I_0=\tau*/\tau_p$, equation (2.57) can be rewritten as

$$Rate_{12}(\delta\tau)=\frac{\eta_1\eta_2}{T_0}\cdot K_{IF}{I_0}^2[1-D_{IF}\mathrm{e}^{-(\delta\tau)^2/{\tau_*}^2}+\tau_*/\tau_p\{1-D_{IF}\mathrm{e}^{-(\delta\tau)^2/{\tau_p}^2}\}]. \qquad (2.59)$$

We show a plot of this function in figure (2.2). The dip consists of two components: a narrow component with width τ_* and a wider, shallow component with width τ_p. Thus we can evaluate these two parameters from the shape of the coincidence count rate curve, much in the same manner as from the SH autocorrelation curve:

$$I_{SH}(\delta\tau)=\frac{K_{SH}}{T_0}\cdot\frac{{I_0}^2}{\tau_p\sqrt{\pi}}(\mathrm{e}^{-(\delta\tau)^2/{\tau_*}^2}+\mathrm{e}^{-(\delta\tau)^2/{\tau_p}^2}), \qquad (2.60)$$

calculated using equations (2.32), (2.45) (2.46), (2.47), and (2.48).

The main difference between the two curves is that the amount of contribution from the τ_p- component relative to the τ_*- component is τ_*/τ_p in the coincidence count rate curve, while they have equal contributions in the SH autocorrelation curve. This is best explained by looking into the origins of the two components, as depicted in figure 2.3. Going back to equation (2.56) we see that the narrow component is caused by a second-order interference effect expressed by $\langle A^*(t_1)\,A(t_1+\delta\tau)\rangle_A$ and $\langle A^*(t_2+\delta\tau)\,A(t_2)\rangle_A$, which occurs only when $|\delta\tau|$ is smaller than the coherence time τ_* (diagrams a-1 and a-2). The duration of this interference with respect to (t_2-t_1) is limited only by the pulse width τ_p. The wider component, corresponding to the product of the correlation functions $\langle A^*(t_1)\,A(t_2)\rangle_A$ and $\langle A^*(t_2+\delta\tau)\,A(t_1+\delta\tau)\rangle_A$, arises from the fact that the fields at the two detectors are correlated when $|t_2-t_1|\le\tau_*$, even when $|\delta\tau|>\tau_*$ (diagrams b-1 and b-2). Therefore its width with respect to $\delta\tau$ is limited only by the pulse width τ_p, while the limitation with respect to (t_2-t_1) results in the coefficient τ_*/τ_p. Observation of this second type of interference requires the use of two photodetectors, and is intrinsically a fourth-order interference effect.

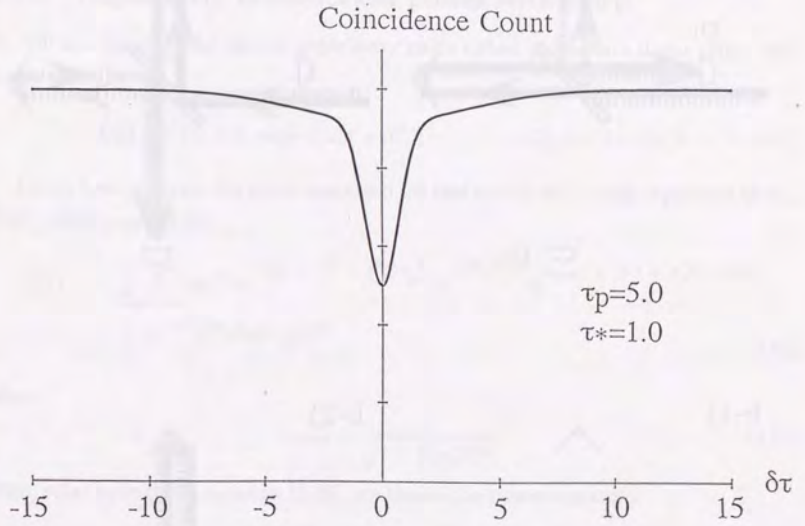

Figure 2.2: Theoretical coincidence count rate curve (2.59) for an imperfectly mode-locked laser, drawn for $\tau_*/\tau_p=0.2$ and $D_{IF}=50\%$. The curve shows a two-component dip at center.

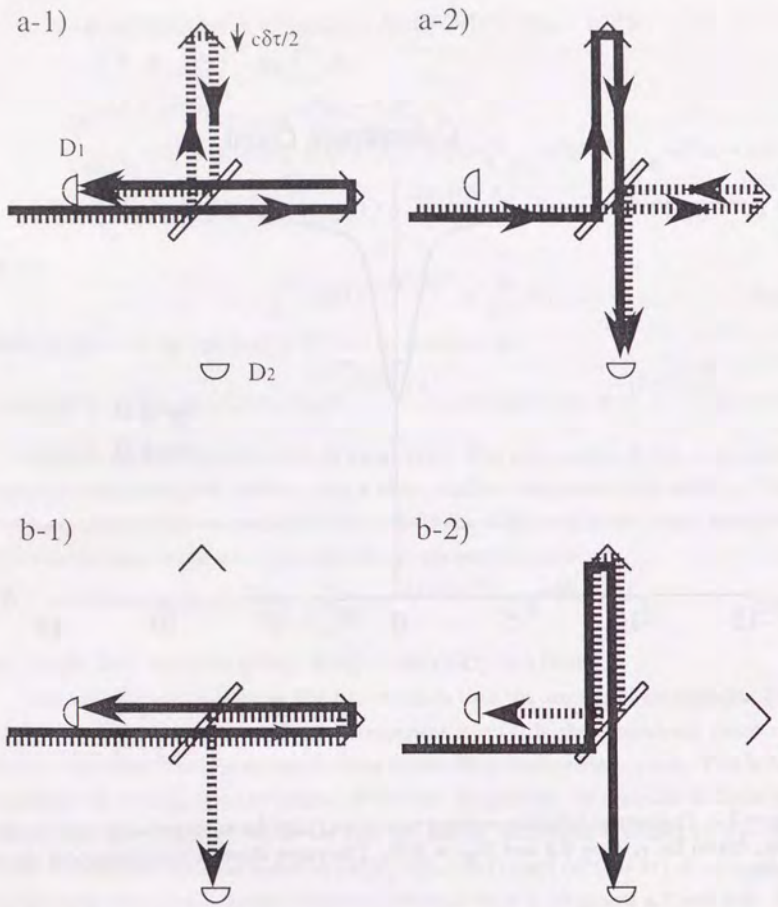

Figure 2.3: Origins of the two components in the coincidence count rate curve (2.59). The various diagrams depict combinations of beam paths that correspond to the fist-order correlation functions of $A(t)$ that appear in equation (2.56): a-1) $\langle A^*(t_1)\,A(t_1+\delta\tau)\rangle_A$; a-2) $\langle A^*(t_2+\delta\tau)\,A(t_2)\rangle_A$; b-1) $\langle A^*(t_1)\,A(t_2)\rangle_A$; b-2) $\langle A^*(t_2+\delta\tau)\,A(t_1+\delta\tau)\rangle_A$.

Lastly let us note that at the limit $\tau_*/\tau_p \to 0$, equation (2.59) coincides with the coincidence count rate curve for the ideally mode-locked case given by equation (2.30).

2.3.4 Imperfectly mode-locked pulses with chirp

We will now consider the case of imperfectly mode-locked pulses with linear chirp. $E(t)$ is now given by

$$E(t) = C(t)\,A(t)\,\exp[-i(\omega_0 t + \beta t^2)] \qquad (-T_0/2 < t < T_0/2) \tag{2.61}$$

Let us first calculate the power spectrum for this new model. Using equations (2.36), (2.47), (2.48), and (2.50),

$$\begin{aligned} R(\tau) &= \frac{1}{T_0}\int_{-\infty}^{\infty} dt C^2\, \mathrm{e}^{-[(t+\tau)^2+t^2]/{\tau_p}^2}\, \mathrm{e}^{-\delta^2\tau^2/2}\, \mathrm{e}^{i[\omega_0\tau+\beta(t+\tau)^2-\beta t^2]} \\ &= \frac{I_0}{T_0}\mathrm{e}^{-\tau^2/2{\tau_{*\,chirp}}^2}\,\mathrm{e}^{i\omega_0\tau}, \end{aligned} \tag{2.62}$$

where

$$\tau_{*\,chirp} = \frac{\tau_*}{\sqrt{1+(\beta\tau_p/\delta)^2}}\,. \tag{2.63}$$

Then, substituting into equation (2.49), we obtain the power spectrum:

$$G(\omega) = \frac{2\pi C^2 \tau_p \tau_{*\,chirp}}{T_0}\,\mathrm{e}^{-{\tau_{*\,chirp}}^2(\omega-\omega_0)^2/2}\,. \tag{2.64}$$

Thus the spectral width is now $1/\tau_{*\,chirp}$. When the parameter $\beta\tau_p/\delta$ is small, $1/\tau_{*\,chirp}$ is close to the original spectral width $1/\tau_*$. As this parameter becomes larger, the spectrum becomes broader than the original. The parameter can be interpreted as the ratio between the amount of frequency shift during a single pulse and the spectral width δ of the fluctuation $A(t)$. In different terms, it is the ratio between the pulse width τ_p and the amount of time δ/β that it takes for the frequency to shift over the original spectral width.

Now we calculate the coincidence count rate for this model. Substituting equation (2.61) into equation (2.22) and using equations (2.45), (2.47), and (2.48), we obtain

$$\begin{aligned} &Rate_{12}(\delta\tau) \\ &= \frac{\eta_1\eta_2}{T_0}\cdot K_{IF}C^4\int_{-\infty}^{\infty}dt_1\int_{-\infty}^{\infty}dt_2 \\ &[\,\mathrm{e}^{2[{t_1}^2+{t_2}^2]/{\tau_p}^2}\{1+\mathrm{e}^{-\delta^2(t_2-t_1)^2}\} \end{aligned}$$

$$-D_{IF}\,\mathrm{e}^{-[t_1^2+(t_2+\delta\tau)^2+t_2^2+(t_1+\delta\tau)^2]/\tau_p^2}\{\mathrm{e}^{-\delta^2(\delta\tau)^2}+\mathrm{e}^{-\delta^2(t_2-t_1)^2}\}$$
$$\mathrm{e}^{i\beta[t_1^2+(t_2+\delta\tau)^2-t_2^2-(t_1+\delta\tau)^2]}]$$
$$=\frac{\eta_1\eta_2}{T_0}\cdot K_{IF}[\,I_0{}^2+I_1I_0-D_{IF}\{I_0{}^2\,\mathrm{e}^{-(\delta\tau)^2/\tau_{*\,chirp}^2}+I_1I_0\,\mathrm{e}^{-(\delta\tau)^2/\tau_{p\,eff}^2}\}], \quad (2.65)$$

where I_0 and I_1 are as given by equations (2.52) and (2.58), and $\tau_{p\ eff}$ is given by

$$\tau_{p\ eff}=\frac{\tau_p}{\sqrt{1+(\beta\tau_p/\delta)^2}}\,. \quad (2.66)$$

From equations (2.52), (2.58), (2.63), and (2.66), we see that

$$\tau_{*\,chirp}/\tau_{p\ eff}=\tau_*/\tau_p=I_1/I_0. \quad (2.67)$$

Therefore, equation (2.65) can be rewritten as:

$$Rate_{12}(\delta\tau)=\frac{\eta_1\eta_2}{T_0}\cdot K_{IF}I_0{}^2[1-D_{IF}\,\mathrm{e}^{-(\delta\tau)^2/\tau_{*\,chirp}^2+\tau_{*\,chirp}/\tau_{p\ eff}}\{1-D_{IF}\,\mathrm{e}^{-(\delta\tau)^2/\tau_{p\,eff}^2}\}]. \quad (2.68)$$

The coincidence count rate curve given by equation (2.68) has the same shape as that given by equation (2.59). The only difference is that τ_* and τ_p are replaced by $\tau_{*\,chirp}$ and $\tau_{p\ eff}$, so that for the same values of τ_* and τ_p, equation (2.68) gives a somewhat narrower dip than equation (2.59).

For comparison let us calculate the SH autocorrelation curve. Using equation (2.32) and the same equations as for the coincidence count rate, we find that the SH autocorrelation curve is the same as that for unchirped pulses:

$$I_{SH}(\delta\tau)=\frac{K_{SH}}{T_0}\cdot\frac{I_0{}^2}{\tau_p\sqrt{\pi}}\,(\mathrm{e}^{-(\delta\tau)^2/\tau_*{}^2}+\mathrm{e}^{-(\delta\tau)^2/\tau_p{}^2}), \quad (2.69)$$

In a chirped pulse, the field corresponding to the front edge of the pulse ceases to interfere with that of the tail part, resulting in a narrowing of the coincidence count rate dip. The SH autocorrelation curve is not altered, however, due to the instantaneous response assumed in equation (2.32). The arguments of E^*'s in equation (2.32) exactly match those of E's, so that the effects of the frequency shift cancel out.

Comparing equations (2.68) and (2.69), we see that the correct value for the pulse width τ_p is given by the SH autocorrelation curve rather than by the coincidence count rate dip. However, the spectral width $1/\tau_{*\,chirp}$ is reflected in the latter rather than the former. The narrow component of the SH autocorrelation measures the "instantaneous" spectral width, "instantaneous" meaning that it is defined for a section of the pulse shorter

than the time δ/β (but longer than τ_*). We also note that the ratio of the widths of the two components remains the same for the SH autocorrelation and the coincidence count rate curves ($\tau_*/\tau_p=\tau_{*\,chirp}/\tau_{p\,eff}$), even for large values of $\beta\tau_p/\delta$.

2.3.5 Perfectly mode-locked pulses with chirp

Let us now consider another type of chirped pulse, where we start with the model for the perfectly mode-locked case and add dispersion:

$$E(t)=\sum_k A_k\exp[i\alpha(k\Delta\omega_{ms})^2]\exp[-i(\omega_0+k\Delta\omega_{ms})t]. \quad (2.70)$$

We take A_k to be real and positive as in subsection 2.3.1, and assume a Gaussian spectrum as in equation (2.28).

Then, for large M we obtain:

$$\begin{aligned}E(t)\ &\sim\ \frac{1}{\Delta\omega_{ms}}\int d\omega\sqrt{K}\exp[-(\omega-\omega_0)^2/4\delta^2]\\ &\quad\exp[i\alpha(\omega-\omega_0)^2]\exp[-i(\omega-\omega_0)t]\exp(-i\omega_0t)\\ &=\ \frac{2\delta\sqrt{\pi K}}{\Delta\omega_{ms}\sqrt{1+\gamma^2}}\,\mathrm{e}^{-\delta^2t^2/(1+\gamma^2)}\,\mathrm{e}^{-i[\omega_0t+\gamma\delta^2t^2/(1+\gamma^2)]}.\end{aligned} \quad (2.71)$$

γ is a measure of the amount of dispersion over the entire spectrum:

$$\gamma=\alpha(2\delta)^2. \quad (2.72)$$

If we define τ_p and C as

$$\tau_p=\frac{\sqrt{1+\gamma^2}}{\delta}\,,\qquad C=\frac{2\delta\sqrt{\pi K}}{\Delta\omega_{ms}\sqrt{1+\gamma^2}}, \quad (2.73)$$

we get:

$$E(t)=C\,\mathrm{e}^{-t^2/\tau_p{}^2}\,\mathrm{e}^{-i[\omega_0t+(\gamma/\tau_p{}^2)t^2]}, \quad (2.74)$$

which is an expression similar to equation (2.61), except that there is no fluctuation represented by $A(t)$. Let us also note that in the present model, the spectral width stays constant and the pulse width becomes larger as the amount of chirp increases. This is in clear contrast with the model given by equation (2.61), where the pulse width stays constant and the spectral width increases. This is because in the present model, the pulse shape is determined as a result of the relationship between the modes, while in equation (2.61) the pulse envelope is given from the outside.

The coincidence count rate for this model can be calculated using equation (2.22):

$$Rate_{12}(\delta\tau) = \frac{\eta_1\eta_2}{T_0} \cdot K_{IF} {I_0}^2 (1 - D_{IF}\, \mathrm{e}^{-(\delta\tau)^2/{\tau_p}^2 {}_{eff}}). \tag{2.75}$$

I_0 is as given by equation (2.52), and $\tau_{p\ eff}$ is given by

$$\tau_{p\ eff} = \frac{\tau_p}{\sqrt{1+\gamma^2}} = \frac{\sqrt{1+\gamma^2}}{\delta} \cdot \frac{1}{\sqrt{1+\gamma^2}} = 1/\delta, \tag{2.76}$$

and is equal to the pulse width for zero dispersion. Thus we see that the width of the coincidence count rate dip stays the same no matter how much dispersion we introduce.

Calculating the SH autocorrelation curve using equation (2.32) for the background-free configuration, we obtain:

$$I_{SH}(\delta\tau) = \frac{K_{SH}}{T_0} \cdot \frac{{I_0}^2}{\tau_p\sqrt{\pi}}\, \mathrm{e}^{-(\delta\tau)^2/{\tau_p}^2}. \tag{2.77}$$

Here again as for the case of imperfectly mode-locked pulses with chirp, we find that the pulse width τ_p is reflected in the SH autocorrelation curve while the coincidence count rate dip given by equation (2.75) and (2.76) gives a correct measure of the spectral width, or, in this case, the pulse width for zero dispersion.

In order to observe the effect of chirp through SH generation (SHG), it is useful to employ a collinear configuration (interferometric SHG) [35] [58]. The SH intensity for this configuration is given by

$$\begin{aligned} I_{SH\,col}(\delta\tau) &= \frac{K_{SH}}{T_0}\int_{-T_0}^{T_0} dt \langle |E(t) + E(t+\delta\tau)|^4 \rangle \\ &= \frac{K_{SH}}{T_0}\int_{-T_0}^{T_0} dt \langle |E(t)|^4 + |E(t+\delta\tau)|^4 + 4|E(t)|^2|E(t+\delta\tau)|^2 \\ &\quad +2(|E(t)|^2 E^*(t)E(t+\delta\tau) + c.c.) \\ &\quad +2(|E(t+\delta\tau)|^2 E^*(t)E(t+\delta\tau) + c.c.) \\ &\quad +(E^{*2}(t)E^2(t+\delta\tau) + c.c.)\rangle. \end{aligned} \tag{2.78}$$

Substituting equations (2.73) and (2.74), we obtain:

$$\begin{aligned} I_{SH\,col}(\delta\tau) &= \frac{K_{SH}}{T_0} \cdot \frac{{I_0}^2}{\tau_p\sqrt{\pi}} 2\Big(1 + 2\,\mathrm{e}^{-(\delta\tau)^2/{\tau_p}^2} \\ &\quad +4\,\mathrm{e}^{-(\frac{3+\gamma^2}{1+\gamma^2})\delta^2(\delta\tau)^2/4} \cos[\omega_0(\delta\tau)] \cos[(\gamma/2{\tau_p}^2)(\delta\tau)^2] \\ &\quad +\mathrm{e}^{-\delta^2(\delta\tau)^2} \cos[2\omega_0(\delta\tau)]\Big). \end{aligned} \tag{2.79}$$

This function has been plotted for two values of γ in figures 2.4 and 2.5. Figure 2.4

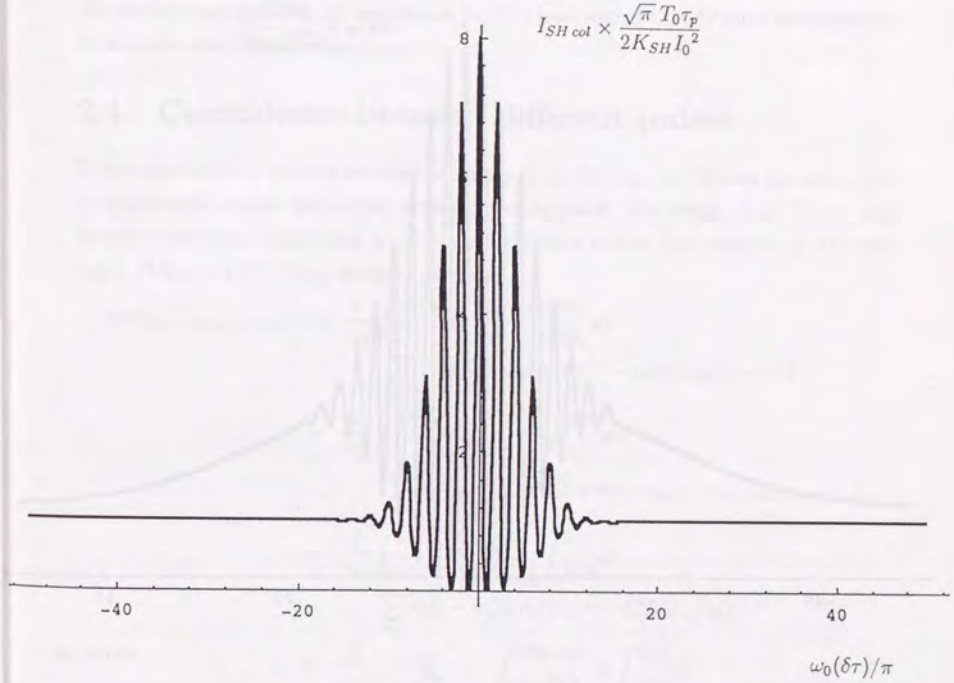

Figure 2.4: SH intensity curve (2.79) for a collinear configuration, for the case of perfectly mode-locked pulses. The curve has been drawn for $\delta/\omega_0 = 1/5\pi$ and $\gamma = 0$ (no chirp).

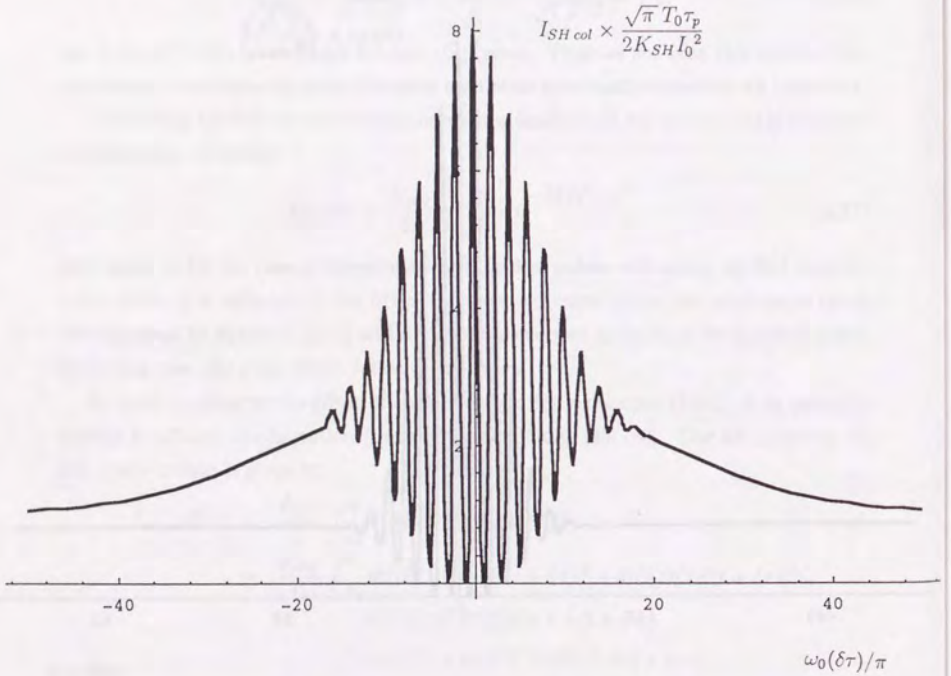

Figure 2.5: SH intensity curve (2.79) for a collinear configuration, for the case of perfectly mode-locked pulses with chirp. The curve has been drawn for $\delta/\omega_0 = 1/5\pi$ and $\gamma = 5$.

corresponds to the case where there is no chirp ($\gamma = 0$), and figure 2.5 corresponds to the chirped case ($\gamma = 5$). We see that the SH intensity is composed by a constant background, a smooth peak whose width is given by τ_p, and an oscillating component whose envelope more or less gives a measure of the inverse of the spectral width. At $\gamma = 0$ the widths of the peak and the oscillating component coincide, but as the dispersion becomes stronger, the tails of the peaked component begin to be visible. We note that pulse measurement by this method requires that the oscillations be fully resolved, so that $\delta\tau$ must be controlled to an order much shorter than $1/\omega_0$.

2.4 Coincidence between different pulses

In previous sections, we have assumed condition (2.11) for τ_{CR}, and limited our discussion to coincidence counts that occur within the same pulse. For longer τ_{CR}, $Rate_{12}$ can include coincidence counts that occur between different pulses. For example, for the case $\tau_{CR} = (2N_{CR}+1)T_0$ (N_{CR}: integer), we have

$$\begin{aligned}
Rate_{12\ (-N_{CR}\ to\ N_{CR})} &\sim \frac{1}{\tau_M}\int_{\tau_0}^{\tau_0+\tau_M} dt \int_{-(N_{CR}+1/2)T_0}^{(N_{CR}+1/2)T_0} d\tau \\
&\quad \sum_{n_1,n_2} \eta_1(t-n_1T_0)\eta_2(t+\tau-n_2T_0)I_{12}(n_2-n_1) \\
&= \frac{1}{\tau_M}\int_{\tau_0}^{\tau_0+\tau_M} dt \sum_{n_3=-N_{CR}}^{N_{CR}} \int_{-T_0/2}^{T_0/2} d\tau \\
&\quad \sum_{n_1,n_2} \eta_1(t-n_1T_0)\eta_2(t+\tau+n_3T_0-n_2T_0)I_{12}(n_2-n_1) \\
&= \frac{1}{\tau_M}\int_{\tau_0}^{\tau_0+\tau_M} dt \sum_{n_3=-N_{CR}}^{N_{CR}} \int_{-T_0/2}^{T_0/2} d\tau \\
&\quad \sum_{n_1} \eta_1(t-n_1T_0)\eta_2(t+\tau-n_1T_0)I_{12}(n_3) \\
&\sim \frac{1}{\tau_M} \sum_{\tau_0<n_1T_0<\tau_0+\tau_M} \int_{n_1T_0-T_0/2}^{n_1T_0+T_0/2} dt \int_{-T_0/2}^{T_0/2} d\tau \\
&\quad \eta_1(t-n_1T_0)\eta_2(t+\tau-n_1T_0) \sum_{n_3=-N_{CR}}^{N_{CR}} I_{12}(n_3) \\
&\sim \frac{1}{\tau_M} N \int_{-T_0/2}^{T_0/2} dt \int_{-T_0/2}^{T_0/2} d\tau \eta_1(t)\eta_2(t+\tau) \sum_{n_3=-N_{CR}}^{N_{CR}} I_{12}(n_3) \\
&= \frac{N}{\tau_M}\eta_1\eta_2 \sum_{n_3=-N_{CR}}^{N_{CR}} I_{12}(n_3) \\
&= \frac{\eta_1\eta_2}{T_0} \sum_{n_3=-N_{CR}}^{N_{CR}} I_{12}(n_3), \qquad (2.80)
\end{aligned}$$

where $I_{12}(n)$ is given by

$$I_{12}(n) = \int_{(1\ \text{pulse})} dt_1 \int_{(1\ \text{pulse})} dt_2 \langle E_1^*(t_1) E_2^*(t_2 + nT_0) E_2(t_2 + nT_0) E_1(t_1) \rangle. \quad (2.81)$$

By changing the interval of integration with respect to τ, we can also measure such quantities as

$$Rate_{12\ (0\ to\ N_{CR})} = \frac{\eta_1 \eta_2}{T_0} \sum_{n_3=0}^{N_{CR}} I_{12}(n_3) \quad (2.82)$$

and

$$Rate_{12\ (n)} = \frac{\eta_1 \eta_2}{T_0} I_{12}(n). \quad (2.83)$$

This last quantity is the rate of coincidence count with the n-th delayed pulse. We will now focus on this quantity, as the others can be calculated as sums over appropriate values of n.

For the interferometer proposed in section 2.2, the rate of coincidence with the n-th delayed pulse is given by:

$$\begin{aligned} &Rate_{12\ (n)}(\delta\tau) \\ &= \frac{\eta_1 \eta_2}{T_0} \cdot K_{IF} \int_{-T_0/2}^{T_0/2} dt_1 \int_{-T_0/2}^{T_0/2} dt_2 \\ &\quad [\langle |E(t_1)|^2 |E(t_2 + nT_0)|^2 \rangle_E \\ &\quad - \frac{D_{IF}}{2} \{ \langle E^*(t_1) E^*(t_2 + nT_0 + \delta\tau) E(t_2 + nT_0) E(t_1 + \delta\tau) \rangle_E \\ &\qquad \cdot \langle \exp[i\{\phi(t_2 + nT_0) - \phi(t_1)\}] \rangle_\phi \\ &\qquad + c.c. \}], \end{aligned} \quad (2.84)$$

where we have distinguished between the average $\langle\ \rangle_\phi$ with respect to $\phi(t)$ and the average $\langle\ \rangle_E$ with respect to fluctuations of the optical field.

From equation (2.84) we immediately see that for very large $|n|$ there will be no dip, since

$$\langle \exp[i\{\phi(t_2 + nT_0) - \phi(t_1)\}] \rangle_\phi = 0. \quad (2.85)$$

For values of n for which the approximation

$$\phi(t_1) \sim \phi(t_2 + nT_0) \quad (2.86)$$

still holds, the behavior of $Rate_{12\ (n)}(\delta\tau)$ is determined by the characteristics of the optical field.

In the case of perfectly mode-locked pulses, it is easily shown from equations (2.26) and (2.27) that

$$E(t + nT_0) = E(t) \exp[-i\omega_0 nT_0], \quad (2.87)$$

and therefore,

$$E^*(t_1) E^*(t_2 + nT_0 + \delta\tau) E(t_2 + nT_0) E(t_1 + \delta\tau) = E^*(t_1) E^*(t_2 + \delta\tau) E(t_2) E(t_1 + \delta\tau). \quad (2.88)$$

Thus we see that for these pulses,

$$Rate_{12\ (n)}(\delta\tau) = Rate_{12\ (0)}(\delta\tau) \quad (2.89)$$

for as long as $\phi(t)$ stays constant.

The behavior of imperfectly mode-locked pulses is a little more complex. Substituting equation (2.46) into equation (2.84) and assuming that

$$C(t + nT_0) = C(t), \quad (2.90)$$

we obtain:

$$\begin{aligned} &Rate_{12\ (n)}(\delta\tau) \\ &= \frac{\eta_1 \eta_2}{T_0} \cdot K_{IF} \int_{-T_0/2}^{T_0/2} dt_1 \int_{-T_0/2}^{T_0/2} dt_2 \\ &\quad [C^2(t_1) C^2(t_2) \langle |A(t_1)|^2 |A(t_2 + nT_0)|^2 \rangle_A \\ &\quad - \frac{D_{IF}}{2} C(t_1) C(t_2 + \delta\tau) C(t_2) C(t_1 + \delta\tau) \\ &\quad \cdot \{ \langle A^*(t_1)\, A^*(t_2 + nT_0 + \delta\tau)\, A(t_2 + nT_0)\, A(t_1 + \delta\tau) \rangle_A + c.c. \}]. \end{aligned} \quad (2.91)$$

In section 2.3 we have implicitly assumed that A_k do not change significantly during a single pulse. Now that we are dealing with coincidence between different pulses, we need to take into account the time dependence of A_k, so that

$$\begin{aligned} &\langle A^*(t_1)\, A^*(t_2 + nT_0 + \delta\tau)\, A(t_2 + nT_0)\, A(t_1 + \delta\tau) \rangle_A \\ &= \langle \sum_{k_1} A_{k_1}^*(t_1)\ \exp[+i\, k_1\, \Delta\omega_{ms}\, t_1] \\ &\quad \sum_{k_2} A_{k_2}^*(t_2 + nT_0 + \delta\tau)\ \exp[+i\, k_2\, \Delta\omega_{ms}\, (t_2 + nT_0 + \delta\tau)] \\ &\quad \sum_{k_3} A_{k_3}(t_2 + nT_0)\ \exp[-i\, k_3\, \Delta\omega_{ms}\, (t_2 + nT_0)] \\ &\quad \sum_{k_4} A_{k_4}(t_1 + \delta\tau)\ \exp[-i\, k_4\, \Delta\omega_{ms}\, (t_1 + \delta\tau)] \rangle_A \\ &= \sum_{k_1,k_2,k_3,k_4} \langle A_{k_1}^*(t_1)\, A_{k_2}^*(t_2 + nT_0 + \delta\tau)\, A_{k_3}(t_2 + nT_0)\, A_{k_4}(t_1 + \delta\tau) \rangle_A \\ &\quad \exp[-i\Delta\omega_{ms}\, \{k_3(t_2 + nT_0) + k_4(t_1 + \delta\tau) - k_1 t_1 - k_2(t_2 + nT_0 + \delta\tau)\}] \\ &= \sum_{k_1,k_2} \langle A_{k_1}^*(t_1)\, A_{k_1}(t_1 + \delta\tau) \rangle_A \langle A_{k_2}^*(t_2 + nT_0 + \delta\tau)\, A_{k_2}(t_2 + nT_0) \rangle_A \\ &\quad \exp[-i\Delta\omega_{ms}\, \{k_1(\delta\tau) - k_2(\delta\tau)\}] \end{aligned}$$

$$+\sum_{k_1,k_2}\langle A^*_{k_1}(t_1)\,A_{k_1}(t_2+nT_0)\rangle_A\langle A^*_{k_2}(t_2+nT_0+\delta\tau)\,A_{k_2}(t_1+\delta\tau)\rangle_A$$
$$\exp[-i\Delta\omega_{ms}\{k_1(t_2+nT_0-t_1)+k_2(t_1-t_2-nT_0)\}]$$
$$-\sum_{k_1}\langle A^*_{k_1}(t_1)\,A^*_{k_1}(t_2+nT_0+\delta\tau)\,A_{k_1}(t_2+nT_0)\,A_{k_1}(t_1+\delta\tau)\rangle_A\,. \quad (2.92)$$

Neglecting the third term for large number of modes M, we obtain:

$$\begin{aligned}
&\langle A^*(t_1)\,A^*(t_2+nT_0+\delta\tau)\,A(t_2+nT_0)\,A(t_1+\delta\tau)\rangle_A\\
&\sim\sum_{k_1}\langle A^*_{k_1}(t_1)\,A_{k_1}(t_1+\delta\tau)\rangle_A\exp[-i\Delta\omega_{ms}\,k_1(\delta\tau)]\\
&\quad\sum_{k_2}\langle A^*_{k_2}(t_2+nT_0+\delta\tau)\,A_{k_2}(t_2+nT_0)\rangle_A\exp[+i\Delta\omega_{ms}\,k_2(\delta\tau)]\\
&\quad+\sum_{k_1}\langle A^*_{k_1}(t_1)\,A_{k_1}(t_2+nT_0)\rangle_A\exp[-i\Delta\omega_{ms}\,k_1(t_2+nT_0-t_1)]\\
&\quad\sum_{k_2}\langle A^*_{k_2}(t_2+nT_0+\delta\tau)\,A_{k_2}(t_1+\delta\tau)\rangle_A\exp[+i\Delta\omega_{ms}\,k_2(t_2+nT_0-t_1)]\\
&=\langle A^*(t_1)\,A(t_1+\delta\tau)\rangle_A\,\langle A^*(t_2+nT_0+\delta\tau)\,A(t_2+nT_0)\rangle_A\\
&\quad+\langle A^*(t_1)\,A(t_2+nT_0)\rangle_A\,\langle A^*(t_2+nT_0+\delta\tau)\,A(t_1+\delta\tau)\rangle_A\,, \quad (2.93)
\end{aligned}$$

or, in terms of $f(\tau)$,

$$\langle A^*(t_1)\,A^*(t_2+nT_0+\delta\tau)\,A(t_2+nT_0)\,A(t_1+\delta\tau)\rangle_A\sim|f(\delta\tau)|^2+|f(t_2+nT_0-t_1)|^2. \quad (2.94)$$

For $T_0\gg\delta\tau$ as was assumed in (2.19),

$$A_k(t+\delta\tau)\sim A_k(t), \quad (2.95)$$

so that

$$\begin{aligned}
f(\delta\tau)&=\sum_k\langle A^*_k(t)\,A_k(t+\delta\tau)\rangle_A\exp[-i\Delta\omega_{ms}\,k(\delta\tau)]\\
&\sim\sum_k\langle A^*_k(t)\,A_k(t)\rangle_A\exp[-i\Delta\omega_{ms}\,k(\delta\tau)], \quad (2.96)
\end{aligned}$$

as given in equation (2.40). On the other hand, for large $|n|$ the phase of $A_k(t+nT_0)$ will have changed randomly from that of $A_k(t)$, so that

$$\langle A^*_k(t_1)\,A_k(t_2+nT_0)\rangle_A\sim\langle A^*_k(t_1)\,A_k(t_2)\rangle_A\exp[-\Gamma_k(nT_0)]. \quad (2.97)$$

The decay rate Γ_k is given roughly by the spectral width of the k-th mode, which is much smaller than $1/T_0$ for well-defined modes. For $|n|\ll 1/(\Gamma_kT_0)$:

$$\begin{aligned}
f(t_2+nT_0-t_1)&=\sum_k\langle A^*_k(t_1)\,A_k(t_2+nT_0)\rangle_A\exp[-i\Delta\omega_{ms}\,k(t_2+nT_0-t_1)]\\
&\sim\sum_k\langle A^*_k(t_1)\,A_k(t_2)\rangle_A\exp[-i\Delta\omega_{ms}\,k(t_2-t_1)]\\
&=f(t_2-t_1), \quad (2.98)
\end{aligned}$$

where equation (2.27) has been used. Then for such n we obtain:

$$\begin{aligned}
&\langle A^*(t_1)\,A^*(t_2+nT_0+\delta\tau)\,A(t_2+nT_0)\,A(t_1+\delta\tau)\rangle_A\\
&\sim|f(\delta\tau)|^2+|f(t_2-t_1)|^2\\
&=\langle A^*(t_1)\,A^*(t_2+\delta\tau)\,A(t_2)\,A(t_1+\delta\tau)\rangle_A, \quad (2.99)
\end{aligned}$$

so that equation (2.89) holds as for perfectly mode-locked pulses.

For the opposite case of $|n|\gg 1/(\Gamma_kT_0)$, we have

$$f(t_2+nT_0-t_1)\sim 0, \quad (2.100)$$

and therefore,

$$\langle A^*(t_1)\,A^*(t_2+nT_0+\delta\tau)\,A(t_2+nT_0)\,A(t_1+\delta\tau)\rangle_A\sim|f(\delta\tau)|^2. \quad (2.101)$$

Substituting into equation (2.91), we obtain:

$$\begin{aligned}
Rate_{12\ (n)}(\delta\tau)&=\frac{\eta_1\eta_2}{T_0}\cdot K_{IF}\int_{-T_0/2}^{T_0/2}dt_1\int_{-T_0/2}^{T_0/2}dt_2[C^2(t_1)C^2(t_2)\\
&\quad-D_{IF}C(t_1)C(t_2+\delta\tau)C(t_2)C(t_1+\delta\tau)|f(\delta\tau)|^2]. \quad (2.102)
\end{aligned}$$

Thus we see that for such n, only the τ_*-component of the dip remains. For other types of pulses, such as fluorescence excited by laser pulse trains, $f(t_2+nT_0-t_1)$ decays more rapidly so that the τ_p-component may disappear even for $n=\pm1$.

Chapter 3

Experiment

In this chapter a description of the light sources and the measurement apparatus will be given, together with an account of the data analysis.

3.1 Lasers

Experiments were performed with two different types of mode-locked lasers, the synchronously pumped Rhodamine 6G dye laser and the self-mode-locked titanium:sapphire laser.

3.1.1 Synchronously pumped Rhodamine 6G dye laser

A synchronously pumped Rhodamine 6G dye laser with group velocity dispersion (GVD) compensation [59] [60] was used to generate imperfectly mode-locked pulses.

Figure 3.1 shows the schematics of the dye laser. A jet of Rhodamine 6G from a 200 μm-thick stainless steel nozzle was synchronously pumped by the second harmonic (SH) of a cw mode-locked Nd^+:YAG (Yttrium Aluminum Garnet) laser (Quantronix Model 416). GVD compensation was provided by a sequence of four BK7 prisms. By adjusting the birefringent filters and the cavity length, the laser can be tuned to various wavelengths and values of τ_s/τ_p. Experiments were performed at wavelength $\lambda \sim 580$ nm and at $\tau_s/\tau_p \sim 1/3$ to $1/5$, where the laser was most stable. The output pulse width was typically of the order of a few picoseconds. The pulse repetition rate was set by the YAG laser to 82 MHz ($T_0 = 12$ ns).

The YAG laser ($\lambda = 1.064$ μm) was operated typically at an output power of around 7 W and pulse width 100 ps. The SH ($\lambda = 532$ nm) was generated by a KTP ($KTiOP_4$) crystal with Type-II phase matching, producing pulses with pulse width 70 ps.

In order to suppress low-frequency fluctuations in the dye laser output power, the YAG laser output power was stabilized by a feedback scheme presented in figure 3.2 [61]. An acousto-optic (AO) modulator for Q-switching is inserted in the laser cavity, in addition to the AO modulator for mode locking. The loss of the Q value created by this additional AO modulator is controlled by feedback of the laser output power in the following way. A very small fraction of the optical field in the YAG laser cavity passes through the end mirror and is detected by a PIN-silicon photodiode. The output voltage of the photodiode is then compared with a stable reference voltage, and the fluctuating component is amplified in the frequency range from 0 to 100 kHZ. This amplified signal is used to modulate the amplitude of the 41 MHz oscillation that drives the AO modulator. The oscillation is modulated in such a way as to increase the cavity loss when the laser output power is

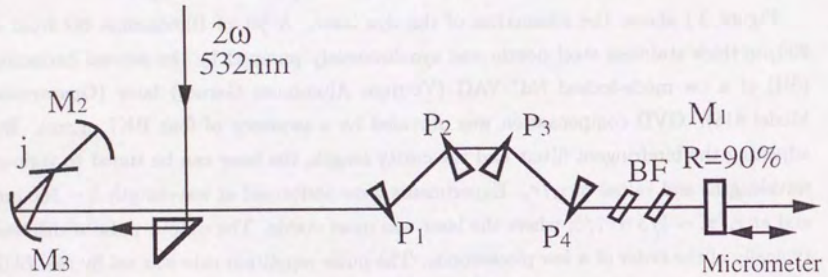

Figure 3.1: Synchronously pumped Rhodamine 6G dye laser with group velocity dispersion compensation:
j, dye jet (Rh6G); M_1, output mirror (R = 90%); P_1, P_2, P_3, P_4, prism sequence for GVD control; M_2, M_3, concave mirrors (f=50) BF, birefringent filters.

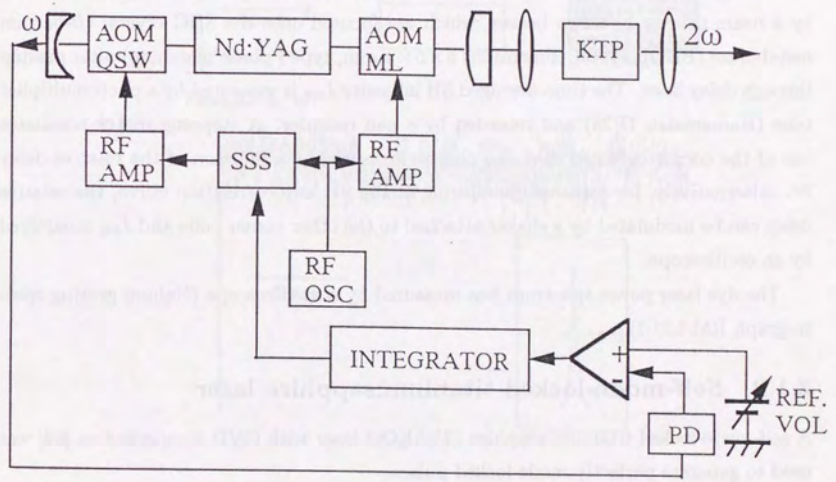

Figure 3.2: Feedback stabilization scheme for the YAG laser:
AOM QSW, AO modulator (Q-switcher); AOM ML, AO modulator (mode-locker); PD, photodiode; SSS, solid state switch (mixer); RF OSC, rf oscillator; RF AMP, rf amplifier.

larger than the target value set by the reference voltage, and vice versa, creating a negative feedback loop.

Figure 3.3 shows the result of this stabilization for the YAG laser and the dye laser. Since the stabilization is realized by the creation of an additional loss in the YAG laser cavity, a slight decrease in output power is inevitable. Thus the output power of the dye laser decreases from 200 mW (without feedback) to 180 mW (with feedback), while the low-frequency fluctuation is suppressed from the original 15% to 5%.

The SH autocorrelation curve for the dye laser output was measured by a background-free configuration shown in figure 3.4. A fraction of the dye laser output is divided by a beam splitter into two beams, which are focused onto the SHG crystal (β-barium metaborate (BBO) crystal, dimensions $5 \times 5 \times 1$ mm, type I phase matching) after passing through delay lines. The time-averaged SH intensity I_{SH} is measured by a photomultiplier tube (Hamamatsu 1P28) and recorded by a pen recorder. A stepping motor translates one of the corner cubes so that I_{SH} can be measured as a function of the relative delay $\delta\tau$. Alternatively, for constant monitoring of the SH autocorrelation curve, the relative delay can be modulated by a shaker attached to the other corner cube and I_{SH} monitored by an oscilloscope.

The dye laser power spectrum was measured by a spectroscope (Nalumi grating spectrograph RM-L21-I).

3.1.2 Self-mode-locked titanium:sapphire laser

A self-mode-locked titanium:sapphire (Ti:Al_2O_3) laser with GVD compensation [62] was used to generate perfectly mode-locked pulses.

Figure 3.5 shows the schematics of the Ti:Al_2O_3 laser. The setup is a modified Spectra-Physics Model 3900 system. The pump laser is a Spectra-Physics Model 2030 argon laser. A sequence of SF6 prisms provided GVD compensation. The laser can be tuned to various wavelengths by adjusting the birefringent filter. Experiments were performed at $\lambda \sim 780$ nm, with typical pulse width of 150 fs. The pulse repetition rate was 82 MHz ($T_0 = 12$ ns).

The SH autocorrelation curve was measured by a collinear configuration shown in figure 3.6. A fraction of the laser output is divided by a beam splitter into two beams, which are focused collinearly onto the SHG crystal (potassium dihydrogen phosphate (KDP) crystal, type I phase matching, 1 mm thickness) after passing through delay lines. The time-averaged SH intensity I_{SH} is measured by a photomultiplier tube and monitored

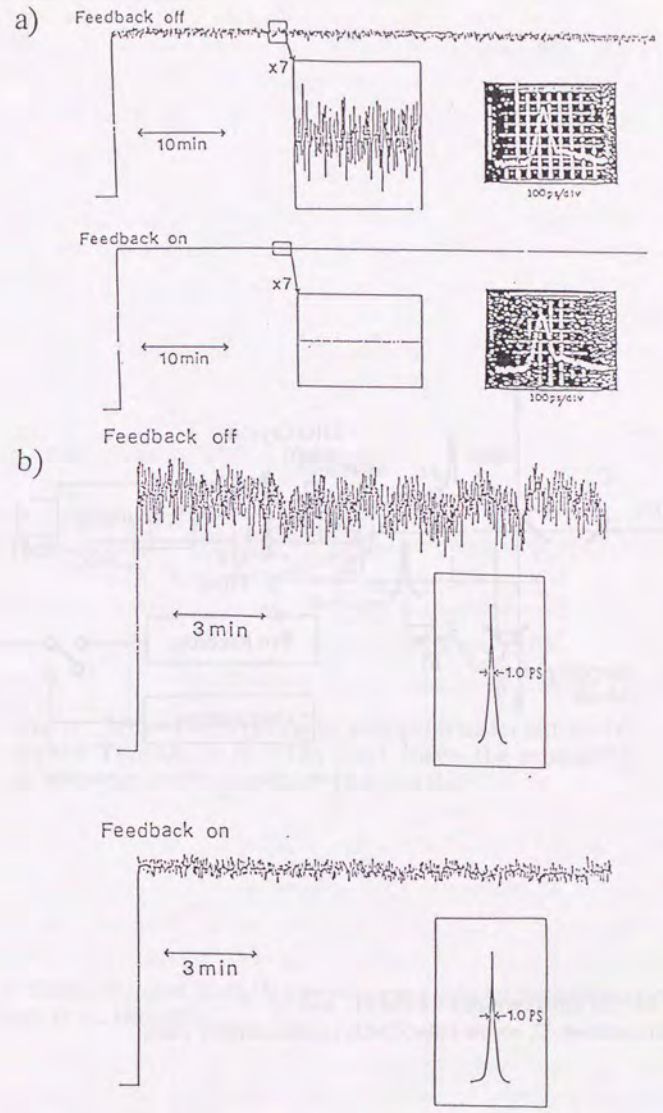

Figure 3.3: Improvement of YAG and dye laser output power stability by the feedback scheme presented in figure 3.2:
a) Output power of the SH of YAG laser with and without feedback stabilization; b) Dye laser output power with and without feedback stabilization to the YAG laser (from Matsumoto *et al.*, 1989 [61]).

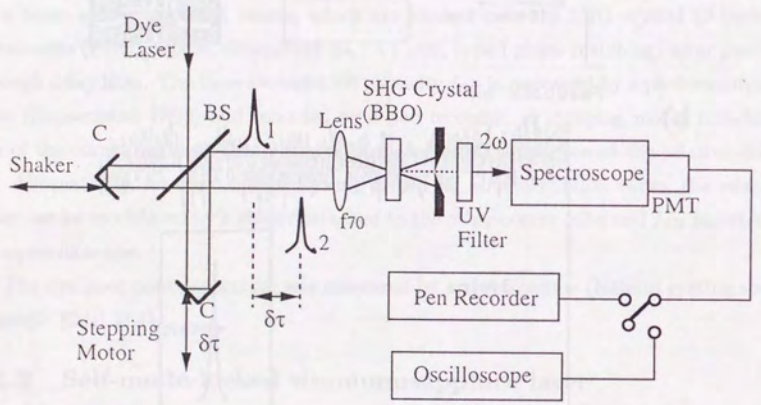

Figure 3.4: SH autocorrelator for the dye laser:
BS, beam splitter; C, corner cube; PMT, photomultiplier tube;

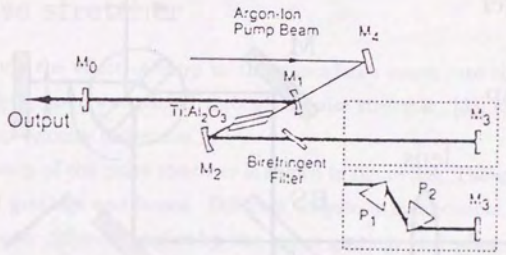

Fig. 1. Schematic of the cavity configuration for self-mode-locked $Ti:Al_2O_3$ laser. The inset shows the intracavity prism sequence for dispersion compensation.

Figure 3.5: Self-mode-locked $Ti:Al_2O_3$ laser with group velocity dispersion compensation (from Spence *et al.*, 1991 [62]).

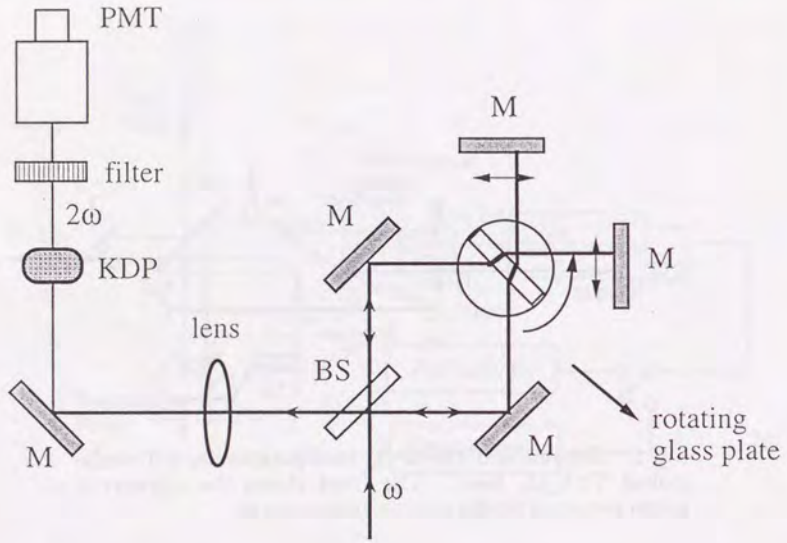

Figure 3.6: SH autocorrelator for the Ti:Al_2O_3 laser:
BS, beam splitter; PMT, photomultiplier tube; M, mirror.

by an oscilloscope. The relative delay is modulated by a rotating glass plate (BK7, 5 mm thickness) inserted near the intersection of the two beams. Delay modulated in this manner is not stable enough to fully resolve the oscillations shown in figures 2.4 and 2.5, but fine enough to resolve the peaked component, thus providing a measure of the pulse width.

The spectral profile was monitored by a simple setup shown in figure 3.7. A fraction of the laser beam is diffracted by a grating, and is focused onto a slit immediately before the photodiode. A rotating glass plate (38 mm thickness) is inserted between the lens and the slit so that different portions of the laser spectrum passes through the slit as the glass plate rotates. Thus the spectral profile of the laser can be obtained by monitoring the output current of the photodiode as a function of time with an oscilloscope.

3.2 Pulse stretcher

In order to study the effect of chirp to the coincidence count rate curve, output pulses from the Ti:Al_2O_3 laser was passed through a pulse stretcher [63] to introduce various degrees of group velocity dispersion.

The schematics of the pulse stretcher is shown in figure 3.8. The stretcher is a simple combination of gratings and lenses. Different frequency components of the input beam are diffracted into different angles by the input grating, and after passing through a telescope-configuration, collected into one beam by the output grating. A simple calculation by geometrical optics shows that the different transit time for the different frequency components result in a group velocity dispersion given by:

$$\frac{d^2\phi}{d\omega^2} = \frac{\lambda^3}{2\pi c^2 s^2 \cos^2\theta_0}(z_1 + z_2), \tag{3.1}$$

where λ is the central frequency, s is the groove spacing of the grating, θ_0 is the emerging angle from the input grating for the central frequency, z_1 and z_2 are as shown in figure 3.8, and the focal lengths of the two lenses were taken to be equal. For $z_1 = z_2 = z$, the setup can be realized using only one grating and lens, by folding back the beam by a mirror as in figure 3.9.

A more detailed analysis shows that there is a spectral lateral walkoff in the stretcher. This effect is compensated by passing the beam through the stretcher a second time, this time in the opposite direction to the first pass.

The pulse stretcher for the present work was constructed according to the folded scheme, and the two pass scheme was used to eliminate spectral lateral walkoff. The

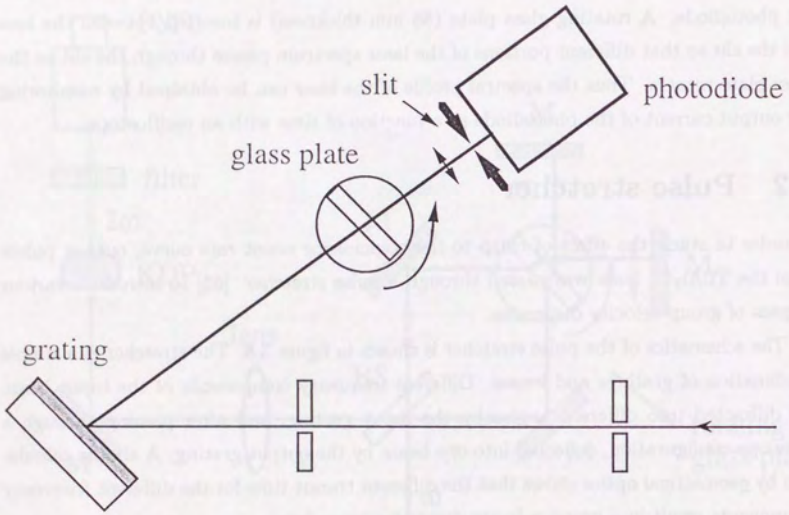

Figure 3.7: Spectrum monitor for the Ti:Al_2O_3 laser.

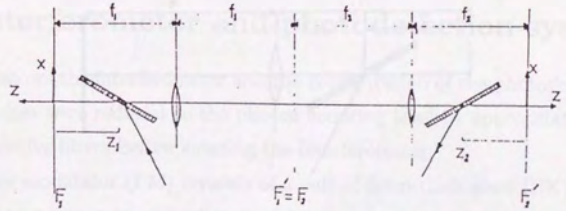

Fig. 1. Scheme of a grating compressor with positive dispersion. The light enters the system through the left hand side grating and exits through the right hand side. z_1 and z_2 are the position of the gratings relative to the focal planes F_1 and F_2', respectively. Such distances are defined negative if the gratings are placed as shown.

Figure 3.8: Schematics of the pulse stretcher (from Martinez, 1987 [63]).

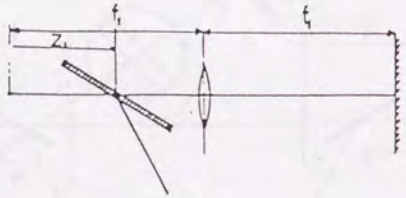

Figure 3.9: Folded scheme for the pulse stretcher (from Martinez, 1987 [63]).

	delay (ns)	τ_{CR} (ns)	coincidence count rate
a)	2	10 - 12	$Rate_{12\ (0)}$
b)	14 -15	10 - 12	$Rate_{12\ (-1)}$
c)	2	50	$Rate_{12\ (0\ to\ -3)}$

Table 3.1: Examples for values of the delay and the coincidence resolution time τ_{CR}, with corresponding coincidence count rates.

grating was a blazed holographic grating ($s = 1/1200$ mm) with 66 % diffraction efficiency at $\lambda = 800$ nm. The focal length of the lens was 400 mm, θ_0 was set around 40°, and z was varied between 0 and -15 mm. For $\lambda \sim 780$ nm, this corresponds to values of $\alpha = (1/2)(d^2\phi/d\omega^2)$ from 0 to $-6.1 \times 10^{-26}\text{sec}^2$.

3.3 Interferometer and photodetection system

Figure 3.10 shows the interferometer and the configuration of the photodetection system. The laser pulses were reduced to the photon counting level by appropriate combinations of neutral density filters before entering the interferometer.

The phase modulator (PM) consists of a pair of 3mm-thick glass (BK7) plates, which are designed to rotate in opposite directions by the same amount and are driven by random electric signals from a chaos generator [64]. In later experiments the glass plates were replaced with 2mm-thick quartz plates. In order to compensate for the optical loss at PM, glass plates are inserted as attenuators in the opposite path (AT). A stepping motor controlled by a computer translates the corner cube C_2.

Photon counting was performed with photomultiplier tubes D_1 and D_2, with typical counting rates of about 10^5 counts per second. The output signals from the two detectors were fed to the start and stop input signal ports of a time-to-amplitude converter (TAC) with delay in the signal line from D_2. Here the time difference between signal arrivals from D_1 and D_2 was measured, and cases where this time difference was shorter than a certain coincidence resolution time τ_{CR} was counted as "coincident".

Figures 3.11 and 3.12 show the distribution of the TAC output for different ranges of signal time difference. In figure 3.12 peaks corresponding to coincidences within the same pulse and those with the first, second, and third delayed pulses can be distinguished. By choosing the combination of the delay and the coincidence resolution time, coincidence count rates corresponding to one or more of these peaks can be measured (table 3.1).

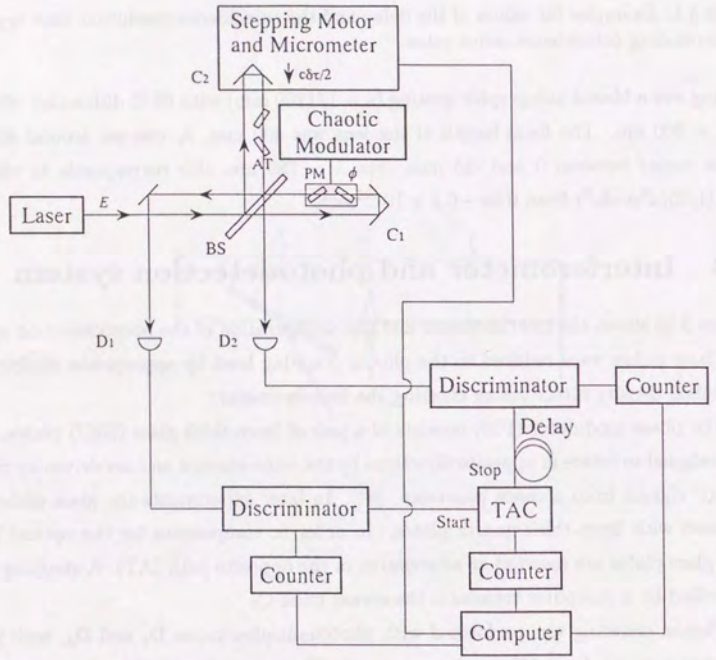

Figure 3.10: Experimental setup for the interferometer and photodetection system: E, input optical field; BS, beam splitter; D_1, D_2, photon-counting detectors; C_1, C_2, corner cubes; PM, phase modulator; AT, attenuator.

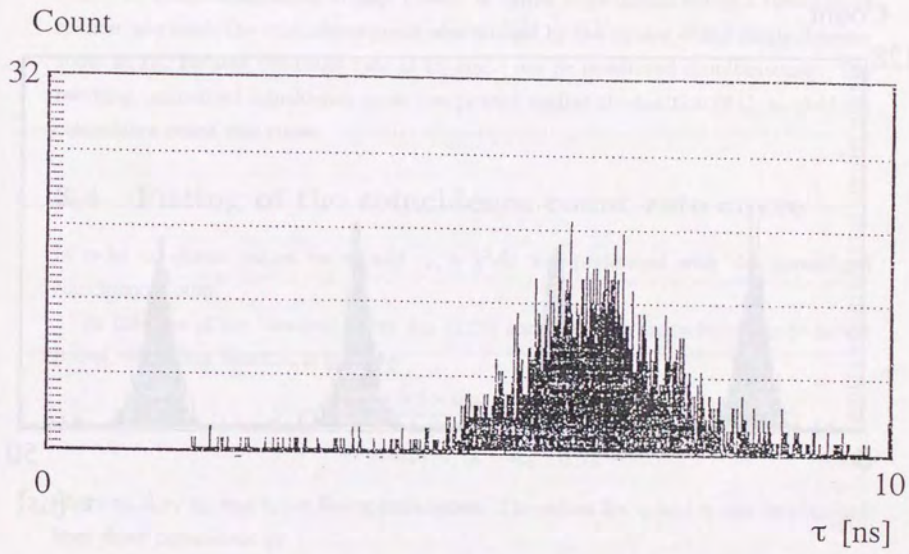

Figure 3.11: TAC output distribution for signal time difference of 0 to 10 ns, with 2 ns delay in the "stop" signal. The peak corresponds to $Rate_{12\ (0)}$ defined in subsection 2.4.

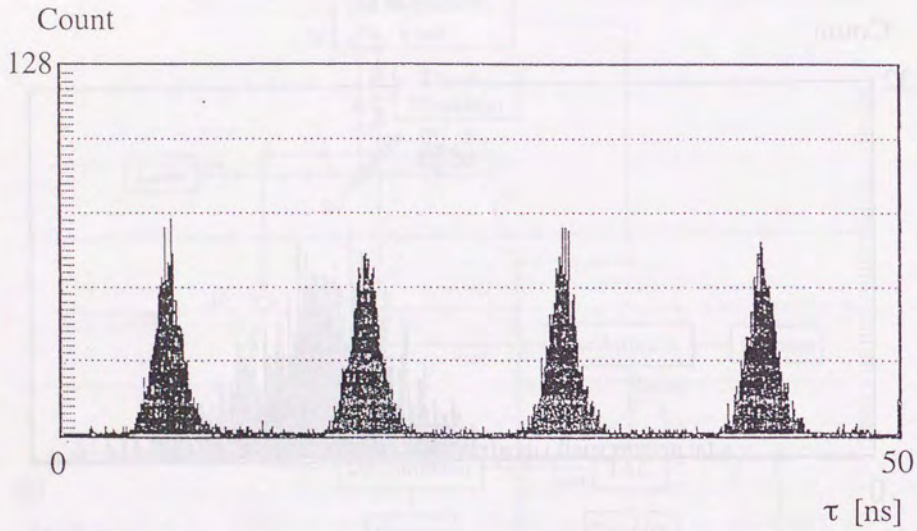

Figure 3.12: TAC output distribution for signal time difference of 0 to 50 ns. with 2 ns delay in the "stop" signal. The peaks correspond from left to right to $Rate_{12\ (0)}$, $Rate_{12\ (-1)}$, $Rate_{12\ (-2)}$, and $Rate_{12\ (-3)}$ defined in subsection 2.4, respectively.

For delay 2 ns and $\tau_{CR} = 10$ to 12 ns, typical coincidence count was 10^4 counts for measurement time 200 sec. From the constant background in the TAC output signal distribution, "accidental coincidence" (mainly due to coincidence between laser pulse and stray light) was estimated to be around 10^3 counts per 200 sec. This value was subtracted from the raw coincidence count, and the result was further divided by the product of the single-detector counting results obtained at D_1 and D_2, in order to eliminate fluctuations caused by minor instabilities in laser power. In earlier experiments where a two-channel counter was used, the coincidence count was divided by the square of the single-detector count at D_2, because the count rate at D_1 could not be monitored simultaneously. The resulting normalized coincidence count was plotted against the position of C_2 to yield the coincidence count rate curve.

3.4 Fitting of the coincidence count rate curve

In order to obtain values for τ_p and τ_*, a χ^2-fit was performed with the normalized coincidence count.

In the case of the two-component dip (2.59) and (2.68) for imperfectly mode-locked pulses, the fitting function is given by

$$\begin{aligned} y &= c_0[1 - \frac{0.5 \times d}{1+r}(\exp[-(x-x_0)^2/t_*^2] \\ &\quad + r \times \exp[-r^2(x-x_0)^2/t_*^2])], \end{aligned} \tag{3.2}$$

where c_0, d, r, x_0, and t_* are fitting parameters. The values for τ_p and τ_* can be obtained from these parameters by:

$$\tau_p = t_*/r, \qquad \tau_* = t_*. \tag{3.3}$$

In the case of the single-component dip (2.30) and (2.75) for perfectly mode-locked pulses, the fitting function is given by

$$y = c_0(1 - 0.5 \times d \times \exp[-(x-x_0)^2/t_*^2]), \tag{3.4}$$

and

$$\tau_p = \tau_* = t_* \tag{3.5}$$

for the unchirped case.

Fitting errors were estimated for parameter values corresponding to [65]

$$\chi^2 = \chi^2_{min} + 1. \tag{3.6}$$

Chapter 4

Experimental Results

This chapter presents results for the experiments described in chapter 3.

4.1 Experimental Results for the dye laser

4.1.1 Basic behavior of $Rate_{12\ (0)}$ and $Rate_{12\ (n)}$

The coincidence count rate for the dye laser pulses were measured with different setups of delay and coincidence resolution time τ_{CR} in order to determine the basic behavior of $Rate_{12\ (0)}$ (delay 2 ns, τ_{CR} 10 ns), $Rate_{12\ (-1)}$ (delay 15 ns, τ_{CR} 10 ns), and $Rate_{12\ (0\ to\ -3)}$ (delay 2 ns, τ_{CR} 50 ns).

The results are plotted in figure 4.1. The three different types of normalized coincidence counts were fitted with the two-component fitting function (3.2) and were divided by the best-fit value of the fitting parameter c_0 (1.15×10^{-10} for $Rate_{12\ (0)}$ and $Rate_{12\ (-1)}$, and 1.14×10^{-9} for $Rate_{12\ (0\ to\ -3)}$) so that they can be compared with one another.

It can be seen that coincidence count rates $Rate_{12\ (0)}$, $Rate_{12\ (-1)}$, and $Rate_{12\ (0\ to\ -3)}$ all behave similarly, and exhibit the same two-component dip predicted by equation (2.59). This is further confirmed by a comparison of the values for τ_* and τ_p obtained by the χ^2-fit (table 4.1). It is shown that coincidence measurement by $Rate_{12\ (0)}$, $Rate_{12\ (-1)}$, and $Rate_{12\ (0\ to\ -3)}$ all give the same values for τ_* and τ_p. This is in accordance with the conclusion in section 2.4 for small values of $|n|$.

These results justify the use of $Rate_{12\ (0\ to\ -3)}$ in place of $Rate_{12\ (0)}$ for measurement of τ_* and τ_p, for the case of the dye laser in this experiment. Such a substitution is especially useful in measurements of very weak or unstable light, because the same number of coincidence counts (and thus the same signal-to-noise ratio) can be obtained in one-fourth the measurement time for $Rate_{12\ (0)}$.

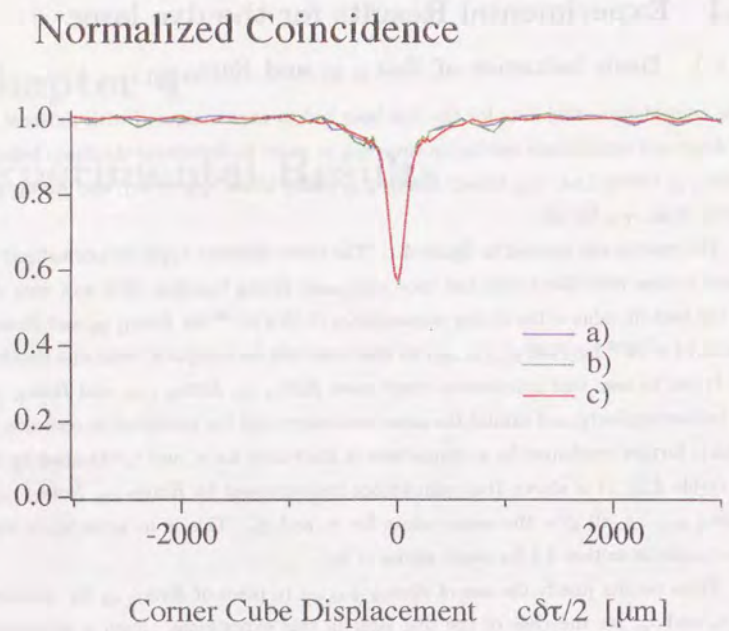

Figure 4.1: Plot of the normalized coincidence counts corresponding to a) $Rate_{12\ (0)}$, b) $Rate_{12\ (-1)}$, and c) $Rate_{12\ (0\ to\ -3)}$ for the dye laser.

delay	τ_{CR}	measured quantity	τ_*	τ_p
2 ns	10 ns	$Rate_{12\ (0)}$	663 ± 7 fs	2.9 ± 0.2 ps
15 ns	10 ns	$Rate_{12\ (-1)}$	649 ± 7 fs	2.9 ± 0.2 ps
2 ns	50 ns	$Rate_{12\ (0\ to\ -3)}$	666 ± 5 fs	3.0 ± 0.1 ps

Table 4.1: Comparison of τ_* and τ_p obtained from normalized coincidence curves corresponding to $Rate_{12\ (0)}$, $Rate_{12\ (-1)}$, and $Rate_{12\ (0\ to\ -3)}$ for the dye laser.

normalized coincidence data	$\tau_*/\tau_p \sim 0.15$	~ 0.2	~ 0.44
reduced χ^2 (2-component fit)	1.324	1.168	0.8176
reduced χ^2 (single-component fit)	10.01	5.485	2.007

Table 4.2: Comparison of reduced χ^2 for the 2-component and single-component fits for the dye laser.

4.1.2 Coincidence count rate curves for different values of τ_*/τ_p.

Figures 4.2, 4.6, and 4.10 give results for the normalized coincidence counts for different values of τ_*/τ_p. The data in figure 4.2 were measured under delay-and-coincidence-resolution setup a) in table 3.1, while those in figures 4.6 and 4.10 were measured under setup c). Corresponding spectral profiles and SH autocorrelation curves are given in figures 4.4 and 4.5, 4.8 and 4.9, and 4.12 and 4.13, respectively.

Figures 4.3, 4.7, and 4.11 compare fitting results with the 2-component fitting function (3.2) and the single-component fitting function (3.4) for the normalized coincidence counts. The 2-component fitting function provides much better fits for all three cases. Respective values of reduced χ^2 (χ^2 normalized by the degrees of freedom) are shown in table 4.2.

It can be seen from the three sets of experimental data how the different values of τ_*/τ_p are reflected in the shapes of the normalized coincidence curves and the SH autocorrelation curves. The deepest dip depth is seen in figure 4.2, where it is 45.3 %. The dips in figures 4.6 and 4.10 are shallower because they were measured without the attenuator AT in figure 3.10.

Tables 4.3, 4.4, and 4.5 compare the values of τ_* and τ_p obtained from the normalized coincidence curve, SH autocorrelation curve, and the spectral profile. In estimating τ_* from the spectral profile, Gaussian spectrum (2.54) was assumed so that $1/\tau_*$ (spectrum width for imperfectly mode-locked pulses) is related to the full-width at half-maximum (FWHM) of the spectral profile $\Delta\nu$ by:

$$1/\tau_* = \frac{\pi}{\sqrt{2\ln 2}}\,\Delta\nu. \tag{4.1}$$

The coefficient in front of $\Delta\nu$ vary for other spectrum shapes.

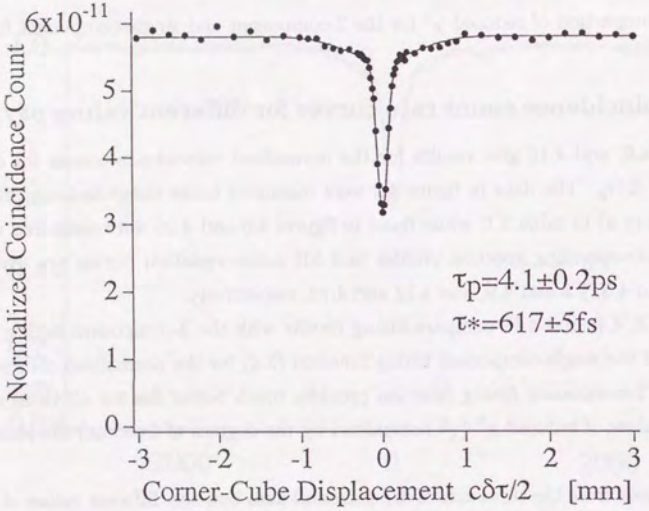

Figure 4.2: Plot of the normalized coincidence count for the dye laser ($\tau_s/\tau_p \sim 0.15$). The dots represent experimental results, and solid line is the theoretical curve with parameters determined to best fit the data. Photon-counting errors are estimated to be of the order of the dot size.

Method of measurement	τ_s	τ_p	$r = \tau_s/\tau_p$
Coincidence count	617 ± 5 fs	4.1 ± 0.2 ps	0.150 ± 0.006
SH autocorrelation	686 ± 3 fs	4.75 ± 0.04 ps	0.1445 ± 0.0006
Spectral profile	660 fs		

Table 4.3: Comparison of τ_s and τ_p obtained by different measurement methods for the dye laser ($\tau_s/\tau_p \sim 0.15$).

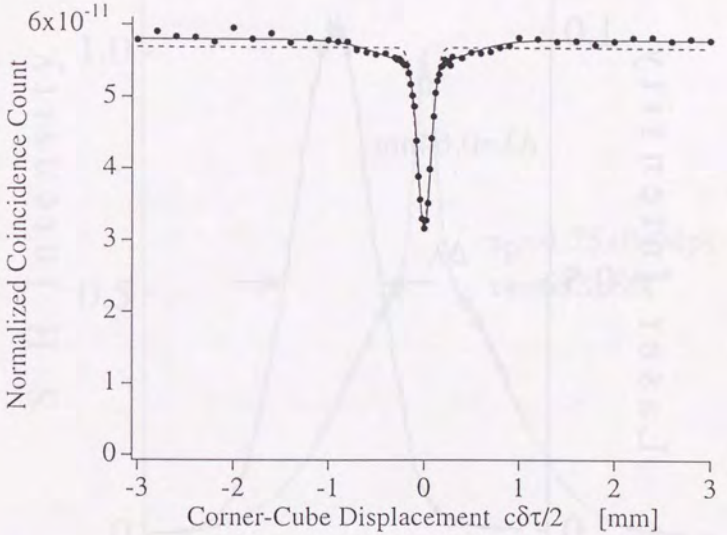

Figure 4.3: Comparison of fitting results with the 2-component fitting function (3.2) (solid line) and the single-component fitting function (3.4) (dashed line) for the normalized coincidence count for the dye laser ($\tau_s/\tau_p \sim 0.15$). The dots represent experimental results. Photon-counting errors are estimated to be of the order of the dot size.

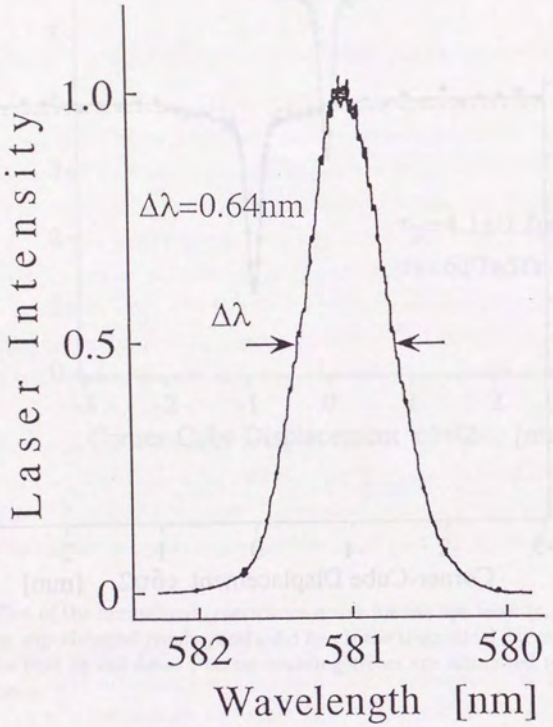

Figure 4.4: Spectral profile for the dye laser ($\tau_* / \tau_p \sim 0.15$).

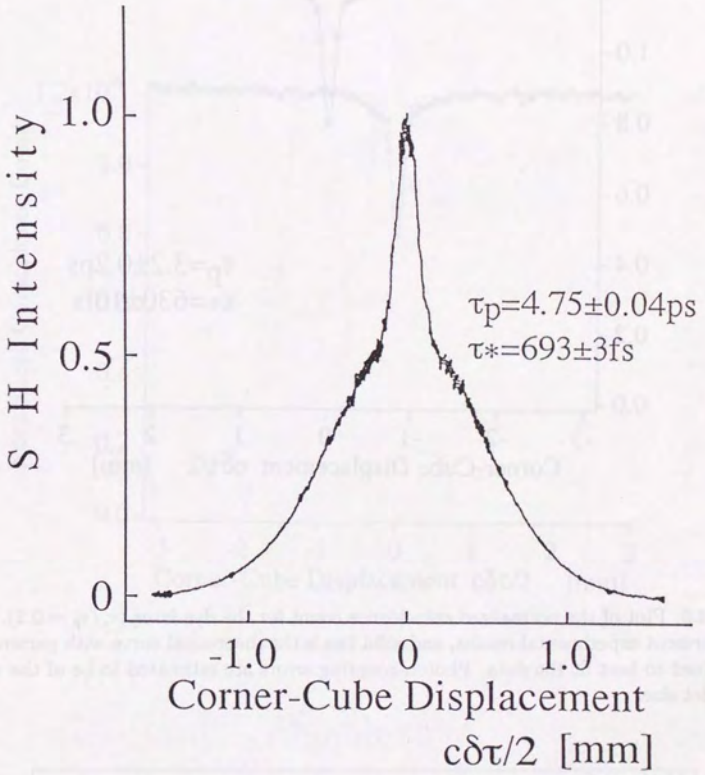

Figure 4.5: SH autocorrelation curve for the dye laser ($\tau_* / \tau_p \sim 0.15$).

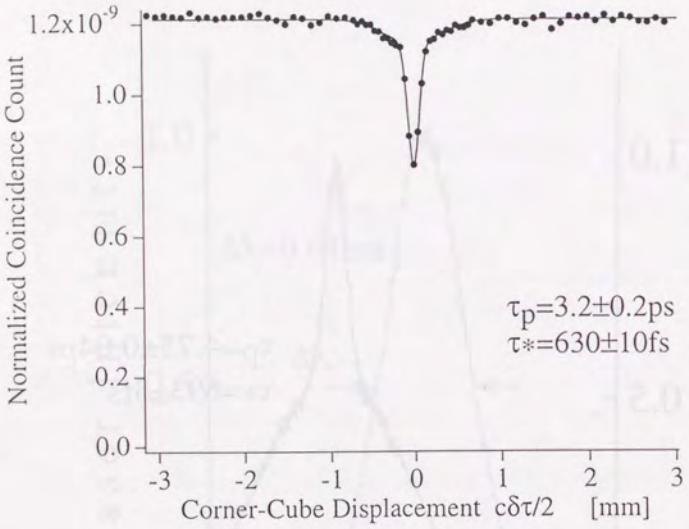

Figure 4.6: Plot of the normalized coincidence count for the dye laser ($\tau_*/\tau_p \sim 0.2$). The dots represent experimental results, and solid line is the theoretical curve with parameters determined to best fit the data. Photon-counting errors are estimated to be of the order of the dot size.

Method of measurement	τ_*	τ_p	$r = \tau_*/\tau_p$
Coincidence count	630 ± 10 fs	3.2 ± 0.2 ps	0.19 ± 0.01
SH autocorrelation	800 ± 3 fs	3.43 ± 0.04 ps	0.233 ± 0.002
Spectral profile	670 fs		

Table 4.4: Comparison of τ_* and τ_p obtained by different measurement methods for the dye laser ($\tau_*/\tau_p \sim 0.2$).

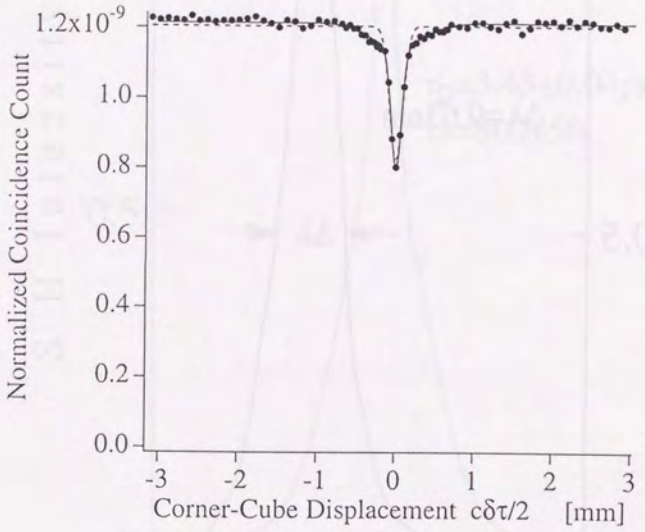

Figure 4.7: Comparison of fitting results with the 2-component fitting function (3.2) (solid line) and the single-component fitting function (3.4) (dashed line) for the normalized coincidence count for the dye laser ($\tau_*/\tau_p \sim 0.2$). The dots represent experimental results. Photon-counting errors are estimated to be of the order of the dot size.

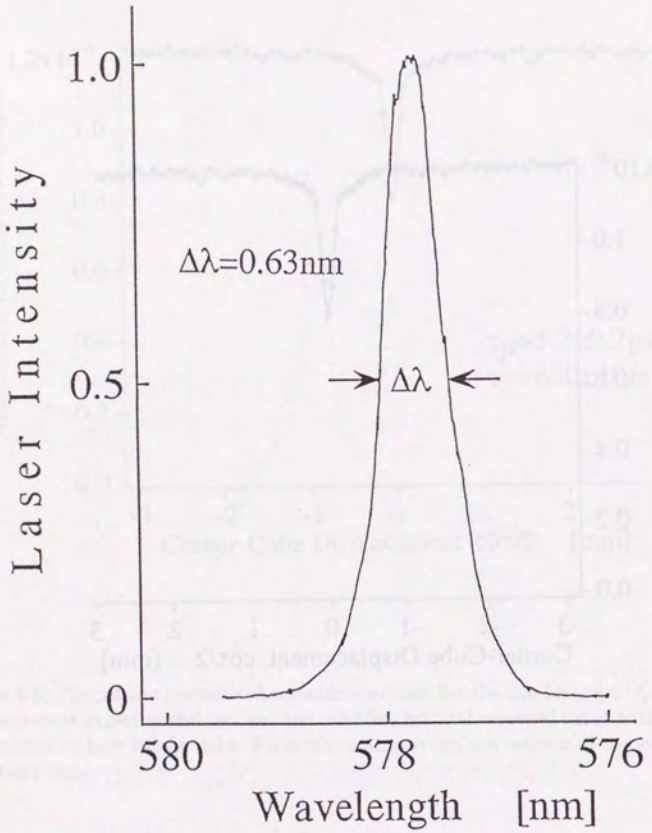

Figure 4.8: Spectral profile for the dye laser ($\tau_s/\tau_p \sim 0.2$).

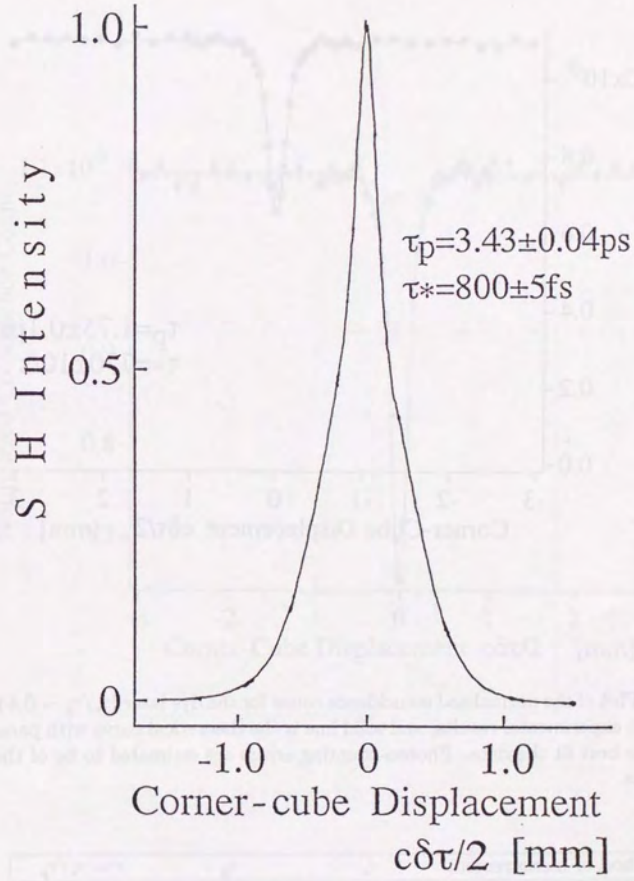

Figure 4.9: SH autocorrelation curve for the dye laser ($\tau_s/\tau_p \sim 0.2$).

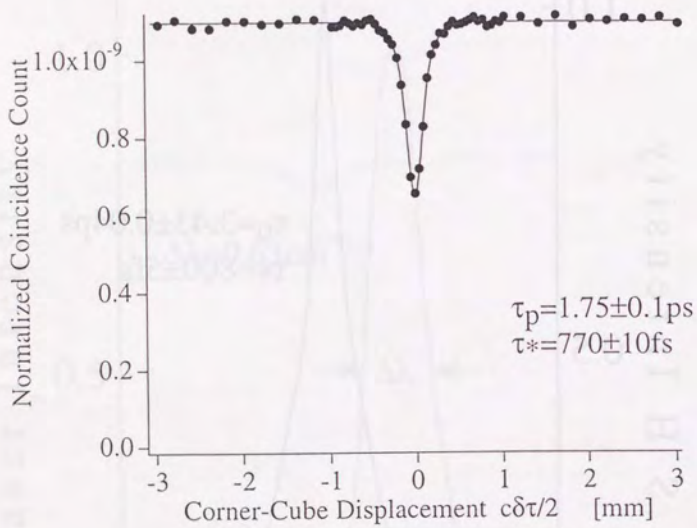

Figure 4.10: Plot of the normalized coincidence count for the dye laser ($\tau_*/\tau_p \sim 0.44$). The dots represent experimental results, and solid line is the theoretical curve with parameters determined to best fit the data. Photon-counting errors are estimated to be of the order of the dot size.

Method of measurement	τ_*	τ_p	$r = \tau_*/\tau_p$
Coincidence count	770 ± 10 fs	1.75 ± 0.1 ps	0.44 ± 0.02
SH autocorrelation	1230 ± 10 fs	2.85 ± 0.07 ps	0.432 ± 0.006
Spectral profile	1020 fs		

Table 4.5: Comparison of τ_* and τ_p obtained by different measurement methods for the dye laser ($\tau_*/\tau_p \sim 0.44$).

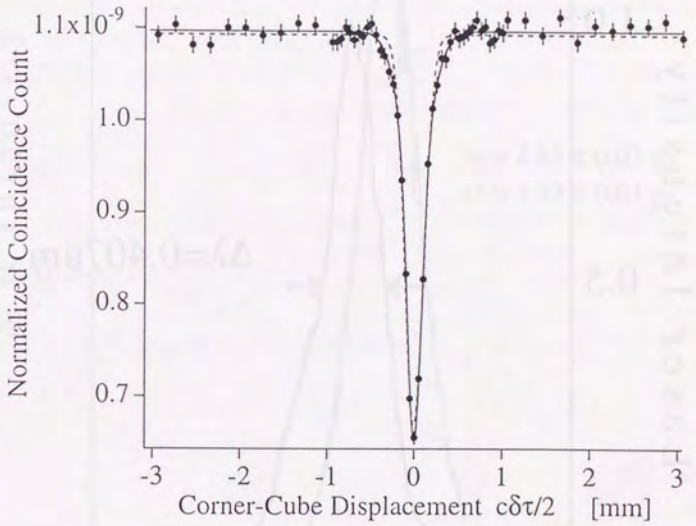

Figure 4.11: Comparison of fitting results with the 2-component fitting function (3.2) (solid line) and the single-component fitting function (3.4) (dashed line) for the normalized coincidence count for the dye laser ($\tau_*/\tau_p \sim 0.44$). The dots represent experimental results.

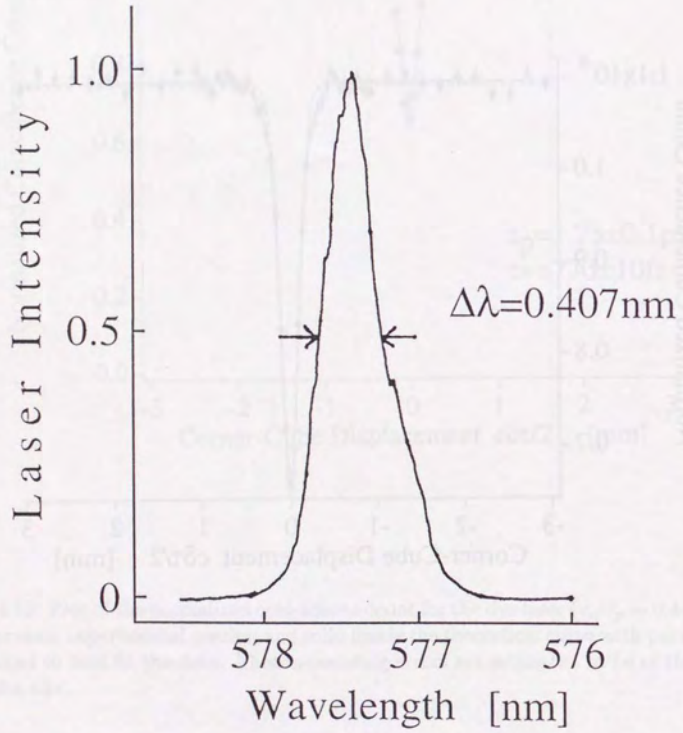

Figure 4.12: Spectral profile for the dye laser ($\tau_* / \tau_p \sim 0.44$).

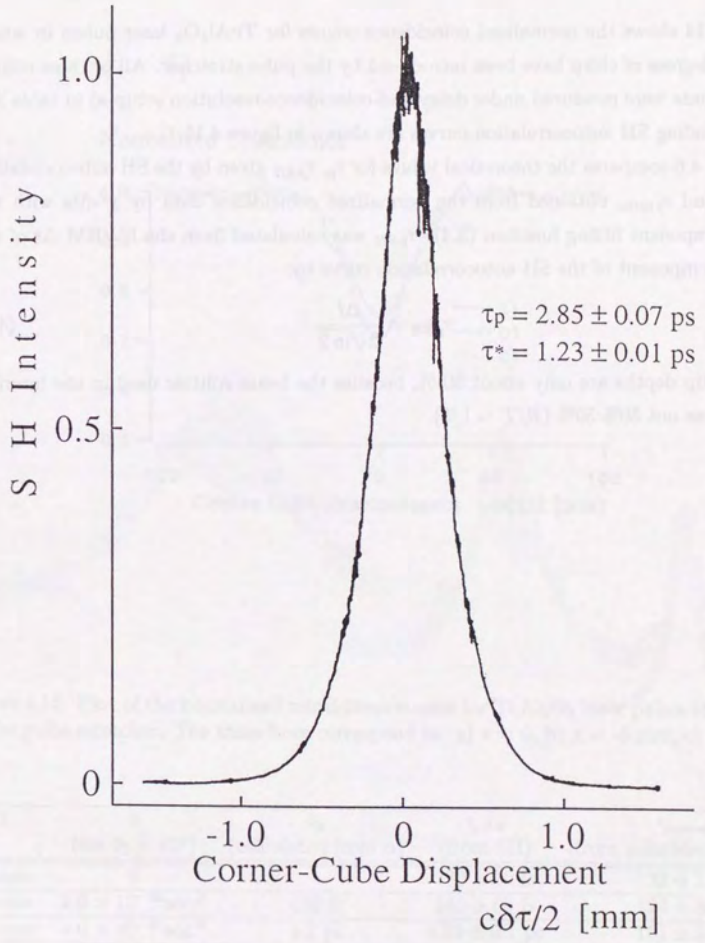

Figure 4.13: SH autocorrelation curve for the dye laser ($\tau_* / \tau_p \sim 0.44$).

4.2 Experimental Results for the titanium:sapphire laser

Figure 4.14 shows the normalized coincidence counts for Ti:Al_2O_3 laser pulses in which varying degrees of chirp have been introduced by the pulse stretcher. All of these coincidence counts were measured under delay-and-coincidence-resolution setup a) in table 3.1. Corresponding SH autocorrelation curves are shown in figure 4.15.

Table 4.6 compares the theoretical values for τ_p, τ_{pSH} given by the SH autocorrelation curves, and τ_{pcoinc} obtained from the normalized coincidence data by χ^2-fits with the single-component fitting function (3.4). τ_{pSH} was calculated from the FWHM Δt of the peaked component of the SH autocorrelation curve by:

$$\tau_{pSH} = \frac{\Delta t}{2\sqrt{\ln 2}}. \tag{4.2}$$

The dip depths are only about 30 %, because the beam splitter used in the interferometer was not 50%:50% ($R/T \sim 1/3$).

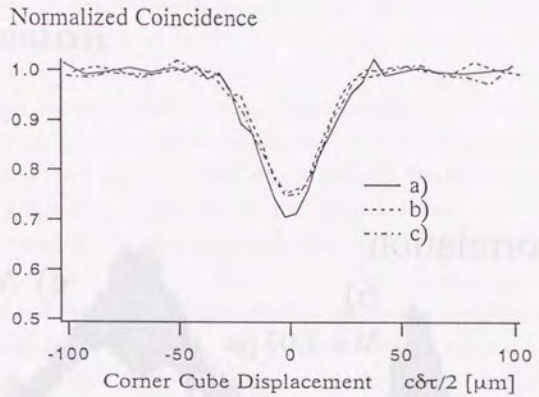

Figure 4.14: Plot of the normalized coincidence counts for Ti:Al_2O_3 laser pulses stretched by the pulse stretcher. The three lines correspond to: a) z = 0, b) z = -5 mm, c) z = -10 mm.

z	α (for $\theta_0 = 40°$)	τ_p (calculated from α)	τ_{pSH} (from SH)	τ_{pcoinc} (from coincidence count)
0 mm	0	–	133 ± 20 fs	132 ± 3 fs
-5 mm	2.0×10^{-26}sec.^{2}	630 fs	645 ± 60 fs	124 ± 3 fs
-10 mm	4.0×10^{-26}sec.^{2}	1.2 ps	1.29 ± 0.1 ps	131 ± 3 fs

Table 4.6: Comparison of theoretical values for τ_p, τ_{pSH} given by the SH autocorrelation curves, and τ_{pcoinc} obtained from the normalized coincidence counts. Theoretical values for τ_p were calculated using equations (2.72) and (2.73), and estimating the value for δ from the inverse of τ_{pSH} at z = 0 mm as 7.5×10^{12} Hz.

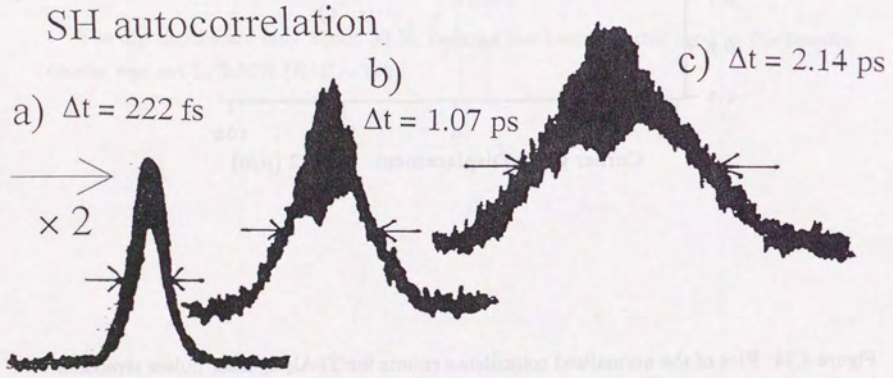

Figure 4.15: SH autocorrelation curves for Ti:Al_2O_3 laser pulses stretched by the pulse stretcher. The three lines correspond to: a) z = 0, b) z = -5 mm, c) z = -10 mm.

Chapter 5

Discussion

This chapter gives a discussion of the experimental results presented in chapter 4, followed by a physical interpretation of the dip and a comparison with the Hanbury-Brown-Twiss experiment.

5.1 Discussion of experimental results

Comparison of the three measurement methods in tables 4.3, 4.4, and 4.5 for the dye laser show that the values for τ_s and τ_p given by the normalized coincidence curves and the SH autocorrelation curves are roughly of the same order. However, closer analysis shows that the values given by the normalized coincidence curves are consistently smaller, while the values for the ratio τ_s/τ_p are about the same for both methods. The values for τ_s given by the spectral profiles fall somewhere in between the other two methods. The best agreement between the three methods has been obtained for the case $\tau_s/\tau_p \sim 0.15$, where the difference between the coincidence counting and the SH autocorrelation methods are within 10 to 15 %.

To some degree, deviations from the Gaussian shape assumed for the spectrum and the pulse envelope in the theoretical model may be responsible for the discrepancies in τ_p and the differences between τ_s given by the normalized coincidence curves and the spectral profiles. However, this still does not explain the differences between τ_s given by the normalized coincidence curves and the SH autocorrelation curves, nor the agreement in the ratio τ_s/τ_p. These features can be explained by the model for imperfectly mode-locked pulses with chirp (equations (2.67), (2.68), and (2.69)). The fact that differences in τ_s between the normalized coincidence curves and the spectral profiles are smaller than those between the normalized coincidence curves and the SH autocorrelation curves may also be considered to support this model (equation (2.64)).

In the case of table 4.6 for the Ti:Al_2O_3 laser interpretation is much more clear. As the amount of chirp increases, the SH autocorrelation curve widens to reflect the longer pulse width, while the width of the coincidence count rate dip constantly gives the pulse width for zero dispersion determined by the inverse of the spectral width. This is exactly as the model for perfectly mode-locked pulses with chirp predicts (equations (2.75), (2.76), and the peaked component of equation (2.79)).

5.2 Origin of the two-component dip

A simple description of the origin of the two-component dip has already been given in chapter 2. This description was given in terms of the first-order correlation functions of $A(t)$, and was thus dependent on the assumption that $A(t)$ obeys Gaussian statistics, *i. e.* that the second-order correlation functions of $A(t)$ can be expressed in terms of the first-order correlation functions. This section attempts to give a more general interpretation in terms of intensity fluctuations.

Generally, in the measurement scheme proposed by this work, two different types of fluctuations are present in the field intensities at the two detectors: the second-order interference fringes modulated by the phase modulator, and the fluctuations of the original input field. It is from these two types of fluctuations that the two-component dip is derived.

Since the two types of fluctuations have completely different origins, they are independent of each other and can be treated separately. The correlation of the latter type of fluctuations can be understood as analogous to that observed in the Hanbury-Brown-Twiss experiment, and is treated in detail in section 5.3. I will now attempt to give a description of the former type of fluctuations.

Let us first write down the expressions for the intensities $|E_1|^2$ and $|E_2|^2$ at the two detectors for $\delta\tau = 0$:

$$|E_1(t_1)|^2 = \frac{1}{2}|E(t_1)|^2 - \frac{1}{2}|E(t_1)|^2 \cos[\phi(t_1)], \tag{5.1}$$

$$|E_2(t_2)|^2 = \frac{1}{2}|E(t_2)|^2 + \frac{1}{2}|E(t_2)|^2 \cos[\phi(t_2)]. \tag{5.2}$$

Here, for simplicity, we have assumed that $R = T = 1/2$ and $T_{PM} = T_{AT} = 1$. We see that the modulations in the two intensities due to the phase modulator are perfectly correlated for small values of $|t_2 - t_1|$; $|E_1|^2$ is maximum when $|E_2|^2$ is minimum, and vice versa. This negative correlation can be understood as the conservation of the total output energy of the interferometer. Because the phase modulator modulates only the phase of the optical field, the total energy that passes through the interferometer is unchanged.

This correlation ceases to exist when $|t_2 - t_1|$ is larger than the time-constant of the modulation. Because this time-constant is much longer than the coincidence resolution time τ_{CR}, contribution from this correlation to the coincidence count rate can be fully resolved and observed. Because the correlation is negative, it leads to a decrease in the coincidence count rate at $\delta\tau = 0$. Multiplying equations 5.1 and 5.2, and averaging over

$\phi(t)$ we get:

$$\begin{aligned}\langle|E_1(t_1)|^2|E_2(t_2)|^2\rangle_\phi &= \frac{1}{4}|E(t_1)|^2|E(t_2)|^2(1-\langle\cos[\phi(t_1)]\cos[\phi(t_2)]\rangle_\phi)\\ &\sim \frac{1}{4}|E(t_1)|^2|E(t_2)|^2(1-\frac{1}{2}),\end{aligned} \tag{5.3}$$

where the last approximation has been made for values of $|t_2-t_1|$ where $\phi(t_1)\sim\phi(t_2)$. Taking the average over intensity fluctuations of the input field we get:

$$\begin{aligned}\langle|E_1(t_1)|^2|E_2(t_2)|^2\rangle_{\phi,E} &\sim \frac{1}{4}\langle|E(t_1)|^2|E(t_2)|^2\rangle_E(1-\frac{1}{2})\\ &= \frac{1}{4}\langle|E(t_1)|^2\rangle_E\langle|E(t_2)|^2\rangle_E[1+\lambda(\delta\tau=0;t_2-t_1)](1-\frac{1}{2})\\ &= \frac{1}{4}\langle|E(t_1)|^2\rangle_E\langle|E(t_2)|^2\rangle_E\\ &\quad[(1-\frac{1}{2})+\lambda(\delta\tau=0;t_2-t_1)(1-\frac{1}{2})].\end{aligned} \tag{5.4}$$

Here $\lambda(\delta\tau=0;t_2-t_1)$ is the correlation of the intensity fluctuations of the original input field.

For $\delta\tau\neq 0$, the depth of the modulation by $\phi(t)$ is determined by the visibility V_i $(i=1,2)$ of the second-order interference fringes given by [5] [6]:

$$\begin{aligned}V_i(\delta\tau) &= \frac{|E_i|^2_{max}-|E_i|^2_{min}}{|E_i|^2_{max}+|E_i|^2_{min}}\\ &= \frac{|\langle E^*(t_i)E(t_i+\delta\tau)\rangle_E|}{\frac{1}{2}[\langle|E(t_i)|^2\rangle_E+\langle|E(t_i+\delta\tau)|^2\rangle_E]},\end{aligned} \tag{5.5}$$

so that now equation (5.4) becomes:

$$\begin{aligned}\langle|E_1(t_1)|^2|E_2(t_2)|^2\rangle_{\phi,E} &\sim \frac{1}{4}\langle|E(t_1)|^2\rangle_E\langle|E(t_2)|^2\rangle_E\\ &\quad[(1-\frac{1}{2}V_1(\delta\tau)V_2(\delta\tau))\\ &\quad+\{\lambda(\delta\tau=0;t_2-t_1)-\frac{1}{2}\lambda(\delta\tau;t_2-t_1)\}],\end{aligned} \tag{5.6}$$

yielding the two-component dip.

In the absence of the intensity fluctuations of the original input field we have:

$$\langle|E_1(t_1)|^2|E_2(t_2)|^2\rangle_{\phi,E}\sim\frac{1}{4}\langle|E(t_1)|^2\rangle_E\langle|E(t_2)|^2\rangle_E(1-\frac{1}{2}V_1(\delta\tau)V_2(\delta\tau)). \tag{5.7}$$

The actual coincidence count rate is obtained by integrating this quantity over t_1 and t_2, but all of the important characteristics are already present. $\frac{1}{4}\langle|E(t_1)|^2\rangle_E\langle|E(t_2)|^2\rangle_E$ is the product of the intensities when there are no interference fringes, and there is a 50 % decrease from this value at $\delta\tau=0$. The width of this decrease is determined by the visibility of the fringes. This applies well to cases of perfectly mode-locked pulses with and without chirp, because these pulses have no intensity fluctuations in excess of the pulse profile. It can be easily understood why in the chirped case the coincidence count rate measures the spectral width rather than the pulse width; it is because the visibility curve is a reflection of the former and not the latter.

5.3 Comparison with the Hanbury-Brown-Twiss experiment

Let us now take a close look at diagrams b-1) and b-2) in figure 2.3, which are related to the τ_p-component of the two-component dip. We see that if we neglect the first transmission/reflection at the beam splitter, the diagrams closely resemble the setup for the Hanbury-Brown-Twiss experiment [1]. Indeed it can be shown that $\lambda(\delta\tau=0;t_2-t_1)$ in section 5.2 is precisely the intensity correlation observed by Hanbury Brown and Twiss. It has been known for the case of stationary light that such a correlation cannot be observed with a slow detector [30]. This section explains why it has been possible to observe this correlation in our case of fast pulses, and how it has led to the measurement of the pulse width.

Figure 5.1 shows the basic setup for the Hanbury-Brown-Twiss experiment. For this type of setup, the fields $E_1(t)$ and $E_2(t)$ at the two detectors D_1 and D_2 can be expressed as

$$E_1(t)=\sqrt{T}\,E(t) \tag{5.8}$$

$$E_2(t)=i\sqrt{R}\,E(t), \tag{5.9}$$

where $E(t)$ is the input field and T and R are the transmittance and the reflectivity of the beam splitter BS. Then, for such $E_1(t)$ and $E_2(t)$ we have

$$\langle|E_1(t_1)|^2|E_2(t_2)|^2\rangle_E=RT\langle|E(t_1)|^2|E(t_2)|^2\rangle_E, \tag{5.10}$$

so that, as in equation (5.4),

$$\langle|E_1(t_1)|^2|E_2(t_2)|^2\rangle_E=RT\langle|E(t_1)|^2\rangle_E\langle|E(t_2)|^2\rangle_E[1+\lambda(\delta\tau=0;t_2-t_1)]. \tag{5.11}$$

The meaning of $\lambda(\delta\tau=0;t_2-t_1)$ becomes clearer if we denote fluctuations in $|E(t)|^2$ by $\Delta|E(t)|^2$ so that

$$|E(t)|^2=\langle|E(t)|^2\rangle_E+\Delta|E(t)|^2. \tag{5.12}$$

Using $\langle \Delta|E(t)|^2\rangle_E = 0$, we obtain:

$$\langle |E_1(t_1)|^2|E_2(t_2)|^2\rangle_E = RT[\langle |E(t_1)|^2\rangle_E\langle |E(t_2)|^2\rangle_E + \langle \Delta|E(t_1)|^2\Delta|E(t_2)|^2\rangle_E]. \quad (5.13)$$

Comparison with equation (5.11) shows that

$$\lambda(\delta\tau = 0; t_2 - t_1) = \frac{\langle \Delta|E(t_1)|^2\Delta|E(t_2)|^2\rangle_E}{\langle |E(t_1)|^2\rangle_E\langle |E(t_2)|^2\rangle_E}. \quad (5.14)$$

Thus $\lambda(\delta\tau = 0; t_2 - t_1)$ is the correlation of the intensity fluctuations normalized by the product of the average intensities.

In the case of the chaotic field described in subsection 2.3.2,

$$\langle |E_1(t_1)|^2|E_2(t_2)|^2\rangle_E = RT[|f(0)|^2 + |f(t_2 - t_1)|^2], \quad (5.15)$$

so that

$$\lambda(\delta\tau = 0; t_2 - t_1) = |f(t_2 - t_1)|^2/|f(0)|^2. \quad (5.16)$$

The width of $\lambda(\delta\tau = 0; t_2 - t_1)$ is directly related to the width of the first-order correlation function $f(t_2 - t_1)$, so that measurement of $\lambda(\delta\tau = 0; t_2 - t_1)$ can give the spectral width of the input field. This is a consequence of the Gaussian statistics expressed in equation (2.45). For other types of fluctuations $\lambda(\delta\tau = 0; t_2 - t_1)$ is not directly related to the first-order correlation functions, but its width can still be considered to be of the order of the coherence time τ_*.

When the detector response is much faster than τ_*, the coincidence count rate between the detectors D_1 and D_2 can be measured as a function of $(t_2 - t_1)$ to directly yield the quantity $\langle |E_1(t_1)|^2|E_2(t_2)|^2\rangle_E$. For slow detection systems equation (5.11) needs to be integrated over the coincidence resolution time τ_{CR}:

$$Rate_{12} \sim \eta_1\eta_2 \int_{-\tau_{CR}/2}^{\tau_{CR}/2} d(t_2 - t_1)\langle |E_1(t_1)|^2|E_2(t_2)|^2\rangle_E. \quad (5.17)$$

For stationary light where $\langle |E(t_1)|^2\rangle_E = \langle |E(t_2)|^2\rangle_E = I$, this gives:

$$\begin{aligned} Rate_{12} &\sim \eta_1\eta_2 RTI^2[\int_{-\tau_{CR}/2}^{\tau_{CR}/2} d(t_2 - t_1) + \int_{-\tau_{CR}/2}^{\tau_{CR}/2} d(t_2 - t_1)\lambda(\delta\tau = 0; t_2 - t_1)] \\ &\sim \eta_1\eta_2 RTI^2\tau_{CR}(1 + \tau_*/\tau_{CR}). \end{aligned} \quad (5.18)$$

Typically τ_{CR} is of the order of nanoseconds, so that for $\tau_* \sim 1$ ps, $\tau_*/\tau_{CR} \leq 10^{-3}$, and for $\tau_* \sim 100$ fs, $\tau_*/\tau_{CR} \leq 10^{-4}$. This means that not only is the shape of the intensity interference term $\lambda(\delta\tau = 0; t_2 - t_1)$ no longer visible, but the coincidence count rate must be determined to the order of $0.1 \sim 0.01$ % before we know if the term exists at all. This

is the reason why intensity correlation of stationary light is difficult to observe with a slow detector.

However, the situation is a little different in the case of pulse trains, because the width of $(\langle |E(t_1)|^2\rangle_E\langle |E(t_2)|^2\rangle_E)$ is limited by the pulse width τ_p. In situations where conditions (2.8) and (2.11) hold (*i. e.* where τ_{CR} is longer than τ_p and τ_* but short enough to distinguish between consecutive pulses), we can utilize equations (2.15) and (2.16) so that:

$$\begin{aligned} Rate_{12} &= \frac{\eta_1\eta_2}{T_0}\int_{-T_0/2}^{T_0/2} dt_1 \int_{-T_0/2}^{T_0/2} dt_2 RT[\langle |E(t_1)|^2\rangle_E\langle |E(t_2)|^2\rangle_E \\ &\quad + \langle |E(t_1)|^2\rangle_E\langle |E(t_2)|^2\rangle_E\lambda(\delta\tau = 0; t_2 - t_1)] \\ &\sim \frac{\eta_1\eta_2}{T_0} \cdot RT(I_p{}^2\tau_p{}^2 + I_p{}^2\tau_p\tau_*) \\ &= \frac{\eta_1\eta_2}{T_0} \cdot RTI_p{}^2\tau_p{}^2(1 + \tau_*/\tau_p), \end{aligned} \quad (5.19)$$

where I_p is the peak intensity. Thus the contribution from the intensity interference term relative to the non-interference term is given by τ_*/τ_p. This means that the intensity interference term can be observed even with a slow detector, as long as $\tau_{CR} \leq T_0$ and the ratio τ_*/τ_p is not too small. In section 2.4 it has been shown that for the case of mode-locked pulses, τ_{CR} can be even longer than T_0. We can say that in the case of fast pulses, the pulse width τ_p plays the role of the effective coincidence resolution time. This is the essence of the ratio τ_*/τ_p between the depths of the τ_p- and τ_*-components of the two-component dip treated in the present work.

In order to clarify the behavior of the intensity interference term for the Michelson-interferometer configuration of the present work, we denote fluctuations in $E^*(t)E(t+\delta\tau)$ by $\Delta(E^*(t)E(t+\delta\tau))$ and rewrite equation (5.3) for $\delta\tau \neq 0$:

$$\begin{aligned} &\langle |E_1(t_1)|^2|E_2(t_2)|^2\rangle_\phi \\ &= \frac{1}{16}[|E(t_1)|^2 + |E(t_1 + \delta\tau)|^2][|E(t_2)|^2 + |E(t_2 + \delta\tau)|^2] \\ &\quad -\frac{1}{16}[E^*(t_1)E(t_1 + \delta\tau)E(t_2)E^*(t_2 + \delta\tau)\langle \exp[i\{\phi(t_2) - \phi(t_1)\}]\rangle_\phi + c.c.] \\ &\sim \frac{1}{16}[|E(t_1)|^2 + |E(t_1 + \delta\tau)|^2][|E(t_2)|^2 + |E(t_2 + \delta\tau)|^2] \\ &\quad -\frac{1}{16}[E^*(t_1)E(t_1 + \delta\tau)E(t_2)E^*(t_2 + \delta\tau) + c.c.] \\ &= \frac{1}{16}[\langle |E(t_1)|^2\rangle_E + \Delta|E(t_1)|^2 + \langle |E(t_1 + \delta\tau)|^2\rangle_E + \Delta|E(t_1 + \delta\tau)|^2] \\ &\quad [\langle |E(t_2)|^2\rangle_E + \Delta|E(t_2)|^2 + \langle |E(t_2 + \delta\tau)|^2\rangle_E + \Delta|E(t_2 + \delta\tau)|^2] \\ &\quad -\frac{1}{16}[\{\langle E^*(t_1)E(t_1 + \delta\tau)\rangle_E + \Delta(E^*(t_1)E(t_1 + \delta\tau))\} \end{aligned}$$

$$\{\langle E(t_2)E^*(t_2+\delta\tau)\rangle_E + \Delta(E(t_2)E^*(t_2+\delta\tau))\} + c.c.]. \quad (5.20)$$

Averaging over fluctuations in $E(t)$ we obtain:

$$\begin{aligned}
&\langle |E_1(t_1)|^2 |E_2(t_2)|^2\rangle_{\phi,E} \\
&\sim \frac{1}{4}\Big[\Big\{\frac{1}{4}(\langle |E(t_1)|^2\rangle_E + \langle |E(t_1+\delta\tau)|^2\rangle_E)(\langle |E(t_2)|^2\rangle_E + \langle |E(t_2+\delta\tau)|^2\rangle_E) \\
&\quad -\frac{1}{2}|\langle E^*(t_1)E(t_1+\delta\tau)\rangle_E||\langle E(t_2)E^*(t_2+\delta\tau)\rangle_E|\Big\} \\
&\quad +\Big\{\frac{1}{4}(\langle \Delta|E(t_1)|^2\Delta|E(t_2)|^2\rangle_E + \langle \Delta|E(t_1+\delta\tau)|^2\Delta|E(t_2+\delta\tau)|^2\rangle_E \\
&\qquad +\langle \Delta|E(t_1)|^2\Delta|E(t_2+\delta\tau)|^2\rangle_E + \langle \Delta|E(t_1+\delta\tau)|^2\Delta|E(t_2)|^2\rangle_E) \\
&\quad -\frac{1}{2}|\langle \Delta(E^*(t_1)E(t_1+\delta\tau))\Delta(E(t_2)E^*(t_2+\delta\tau))\rangle_E|\Big\}\Big] \\
&\sim \frac{1}{4}\Big[\Big\{\langle |E(t_1)|^2\rangle_E\langle |E(t_2)|^2\rangle_E \\
&\quad -\frac{1}{2}|\langle E^*(t_1)E(t_1+\delta\tau)\rangle_E||\langle E(t_2)E^*(t_2+\delta\tau)\rangle_E|\Big\} \\
&\quad +\Big\{\langle \Delta|E(t_1)|^2\Delta|E(t_2)|^2\rangle_E \\
&\quad -\frac{1}{2}|\langle \Delta(E^*(t_1)E(t_1+\delta\tau))\Delta(E(t_2)E^*(t_2+\delta\tau))\rangle_E|\Big\}\Big], \quad (5.21)
\end{aligned}$$

where, in the last approximation, we have neglected minor details that do not show in the final integrated result. Comparison with equation (5.6) shows that the term $\lambda(\delta\tau; t_2-t_1)$, which determines the behavior of the intensity-interference component at $\delta\tau \neq 0$, is given by:

$$\lambda(\delta\tau; t_2-t_1) = \frac{|\langle \Delta(E^*(t_1)E(t_1+\delta\tau))\Delta(E(t_2)E^*(t_2+\delta\tau))\rangle_E|}{\frac{1}{4}(\langle |E(t_1)|^2\rangle_E + \langle |E(t_1+\delta\tau)|^2\rangle_E)(\langle |E(t_2)|^2\rangle_E + \langle |E(t_2+\delta\tau)|^2\rangle_E)}. \quad (5.22)$$

$\langle \Delta(E^*(t_1)E(t_1+\delta\tau))\Delta(E(t_2)E^*(t_2+\delta\tau))\rangle_E$ is not as sensitive to $\delta\tau$ as $\langle E^*(t)E(t+\delta\tau)\rangle_E$, because at $|t_2-t_1| < \tau_*$ phase fluctuations in $\Delta(E^*(t_1)E(t_1+\delta\tau))$ are mostly canceled by $\Delta(E(t_2)E^*(t_2+\delta\tau))$. However, it is still required that the two pulses $E(t)$ and $E(t+\delta\tau)$ overlap, so that the width of $\lambda(\delta\tau; t_2-t_1)$ with respect to $\delta\tau$ is limited by the pulse width τ_p. It is by taking advantage of this behavior that the present work has succeeded in measuring τ_p.

An experiment similar to the present work has been performed with the off-axis fluorescence from laser dye by Ou *et al.* [55]. In their work, terms corresponding to $\lambda(\delta\tau = 0; t_2-t_1)$ and $\lambda(\delta\tau; t_2-t_1)$ have been neglected, because the light source was stationary and contributions from these terms were too small to be observed. Therefore their experiment purely measured the modulation of the second-order interference fringes by the phase modulator. In our experiment with fast pulses, the pulse width has acted as

the effective coincidence resolution, so that not only the modulation by the phase modulator but also the intensity fluctuations of the original input field has been observed. The behavior of the former with respect to $\delta\tau$ has led to the measurement of the coherence time, while that of the latter has enabled the measurement of the pulse width.

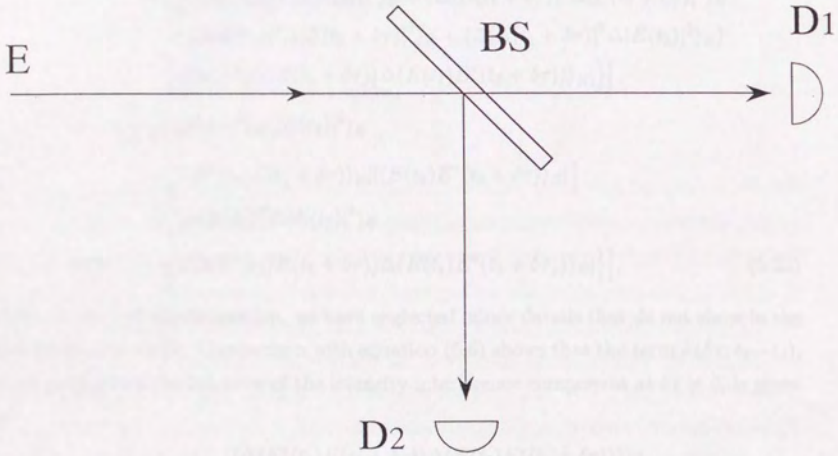

Figure 5.1: Scheme for the Hanbury-Brown-Twiss experiment:
E, input optical field; BS, beam splitter; D_1, D_2, photodetectors.

Chapter 6

Conclusion

It has been demonstrated both theoretically and experimentally that by combining a Michelson-interferometer configuration and the coincidence-counting method, simultaneous measurement of the pulse width and coherence time of fast laser pulses is possible. A time resolution much smaller than the detector response time has been obtained.

This is the first observation of a systematic temporal variation of the intensity of light through intensity interference. Physically, this has been made possible through observation of the correlation of the intensity fluctuations of the original input field, which similar experiments with stationary light have not been able to observe with a slow detector.

Since the method does not require a nonlinear medium, it is applicable to a wide range of frequency regions, including regions where no appropriate SH crystal is available. The method is based on photon counting, so it can be applied to measurement of weak light sources such as fluorescence.

Through comparison with the conventional SH autocorrelation method, it has been revealed that this new method behaves differently towards incoherent pulse broadening caused by imperfect locking of the laser modes, and coherent pulse broadening of chirped pulses. It is an interesting feature of the new method that it distinguishes between the two types of pulse broadenings and reflects only the former.

This characteristic implies that in situations where we do not wish to distinguish between the two types of broadenings, but are interested in pulse width as purely a temporal distribution of the intensity of light, the SH autocorrelation method is a better choice. However, in situations where interest is in the physical phenomena that determine the pulse width *before* broadening by group velocity dispersion sets in, the intensity interference method can be a useful tool. Especially, it allows one to make measurements without influence from group velocity dispersion introduced by the optical elements in the interferometer, which can be a problem in the measurement of femtosecond pulses by the SH autocorrelation method.

It is also possible to combine the present method with the SH autocorrelation method to determine the amount of chirp in the measured pulse. Conventionally this has been realized through comparison of the spectral width with the width of the SH autocorrelation curve, or through SH autocorrelation measurement with a collinear configuration (interferometric SHG). The former involves a conversion of information in the frequency domain to the time domain, so a precise measurement of the shape of the spectral profile is necessary in order to obtain a time-constant that can be compared with the width of

the SH autocorrelation curve. The latter method requires that the time-delay can be controlled to an order much shorter than the wavelength. The method proposed in the present work has the advantage that it directly produces information in the time-domain which can be compared with the width of the SH autocorrelation curve, and that the requirement on time-delay control is not so strict.

Acknowledgement

Firstly I would like to thank my advisor Professor Masahiro Matsuoka, who has first pointed me to this theme and whose encouragement and long experience with quantum optics has been valuable throughout.

I owe much to my collaborators: Professor Takahiro Kuga who has given me a basic training in various experimental techniques and helped me design the original interferometer, and Dr. Motoyoshi Baba whose help with the dye laser and in refinement of the experimental apparatus has been valuable indeed. Ying Li's research on the application of the method to measurement of fluorescence and scattered light provided much insight. Stimulating discussions with the members, both former and present, of the Matsuoka Group has helped me overcome various theoretical and experimental problems. Thank you all.

I would also like to thank Professors Shuntaro Watanabe, Hiroto Kuroda, and Tohru Suemoto, and the other members of the Laser Group at the Institute for Solid State Physics, for active discussions and a friendly atmosphere. I thank especially: Dr. Koichiro Tanaka, for help with the titanium sapphire laser and for pointing me to various literature; Hideyuki Ohtake, for also helping me with the titanium sapphire laser; Dr. Kiminori Kondo, Yasuo Nabekawa, and Jiro Itatani, for help with the pulse stretcher.

Finally I would like to thank my husband Takashi Miyamoto for the emotional support and for providing a closest example of the viewpoint of a physicist in a different genre.

Bibliography

[1] R. Hanbury Brown and R. Q. Twiss, "Correlations between photons in two coherent beams of light", Nature **177**, 27 (1956).

[2] R. Hanbury Brown and R. Q. Twiss, "A test of a new type of stellar interferometer on Sirius", Nature **178**, 1046 (1956).

[3] R. Hanbury Brown and R. Q. Twiss, "Interferometry of the intensity fluctuations in light, I. Basic theory: the correlation between photons in coherent beams of radiation ", Proc. R. Soc. A **242**, 300 (1957).

[4] R. Hanbury Brown and R. Q. Twiss, "Interferometry of the intensity fluctuations in light, II. An experimental test of the theory for partially coherent light", Proc. R. Soc. A **243**, 291 (1958).

[5] M. Born and E. Wolf, *Principles of optics, fifth ed.*, (Pergamon Press, Oxford, 1975).

[6] R. Loudon, *The quantum theory of light*, (Clarendon Press, Oxford, 1973).

[7] R. J. Glauber, "The quantum theory of optical coherence", Phys. Rev. **130**, 2529 (1963).

[8] R. J. Glauber, "Optical coherence and photon statistics", in *Quantum optics and electronics*, edited by C. DeWitt, A. Blandin, and C. Cohen-Tannoudji (Gordon and Breach, New York, 1965).

[9] R. J. Glauber, "Coherent and Incoherent States of the Radiation Field", Phys. Rev. **131**, 2766 (1963).

[10] R. Q. Twiss, A. G. Little, and R. Hanbury Brown, "Correlation between photons, in coherent beams of light, detected by a coincidence counting technique", Nature **180**, 324 (1957).

[11] G. A. Rebka and R. V. Pound, "Time-correlated photons", Nature **180**, 1035 (1957).

[12] L. Mandel and E. Wolf, "Coherence properties of optical fields", Rev. Mod. Phys. **37**, 231 (1965).

[13] W. Martienssen and E. Spiller, "Coherence and fluctuations in light beams", Am. J. Phys. **32**, 919 (1964).

[14] F. T. Arecchi, "Measurement of the statistical distribution of Gaussian and laser sources", Phys. Rev. Lett. **15**, 912 (1965).

[15] F. T. Arecchi, E. Gatti, and A. Sona, "Time distribution of photons from coherent and Gaussian sources", Phys. Lett. **20**, 27 (1966).

[16] B. L. Morgan and L. Mandel, "Measurement of photon bunching in a thermal light beam", Phys. Rev. Lett. **16**, 1012 (1966).

[17] R. L. Pfleegor and L. Mandel, "Interference of independent photon beams", Phys. Rev. **159**, 1084 (1967).

[18] R. L. Pfleegor and L. Mandel, "Further experiments on interference of independent photon beams at low light levels", J. Opt. Soc. Am. **58**, 946 (1968).

[19] L. Mandel, E. C. G. Sudarshan, and E. Wolf, "Theory of photoelectric detection of light fluctuations", Proc. Phys. Soc. **84**, 435 (1964).

[20] H. J. Kimble, M. Dagenais, and L. Mandel, "Photon antibunching in resonance fluorescence", Phys. Rev. Lett. **39**, 691 (1977).

[21] E. Jakeman, E .R. Pike, P. N. Pusey, and J. M. Vaughan, "The effect of atomic number fluctuations on photon antibunching in resonance fluorescence", J. Phys. A **10**, L257 (1977).

[22] R. Short and L. Mandel, "Observation of sub-Poissonian photon statistics", Phys. Rev. Lett. **51**, 384 (1983).

[23] F. Diedrich and H. Walther, "Nonclassical radiation of a single stored ion", Phys. Rev. Lett. **58**, 203 (1987).

[24] L. Mandel, "Photon interference and correlation effects produced by independent quantum sources", Phys. Rev. A **28**, 929, (1983).

[25] H. Paul, "Interference between independent photons", Rev. Mod. Phys. **58**, 209 (1986).

[26] R. Ghosh, C. K. Hong, Z. Y. Ou, and L. Mandel, "Interference of two photons in parametric down conversion", Phys. Rev. A **34**, 3962 (1986).

[27] R. Ghosh and L. Mandel, "Observation of nonclassical effects in the interference of two photons", Phys. Rev. Lett. **59**, 1903 (1987).

[28] E. Brannen and H. I. S. Ferguson, "The question of correlation between photons in coherent light rays", Nature **178**, 481 (1956).

[29] R. Hanbury Brown and R. Q. Twiss, "The question of correlation between photons in coherent light rays", Nature **178**, 1447 (1956).

[30] E. M. Purcell, "The question of correlation between photons in coherent light rays", Nature **178**, 1449 (1956).

[31] J. A. Giordmaine, P. M. Rentzepis, S. L. Shapiro, and K. W. Wecht, "Two-photon excitation of fluorescence by picosecond light pulses", Appl. Phys. Lett. **11**, 216 (1967).

[32] J. A. Armstrong, "Measurement of picosecond laser pulse widths", Appl. Phys. Lett. **10**, 16 (1967).

[33] R. C. Eckardt and C. H. Lee, "Optical third harmonic measurements of subpicosecond light pulses", Appl. Phys. Lett. **15**, 425 (1969).

[34] *Ultrashort Light Pulses, second ed.*, edited by S. L. Shapiro, (Springer-Verlag, Berlin, 1984).

[35] *Ultrashort Laser Pulses, second ed.*, edited by W. Kaiser, (Springer-Verlag, Berlin, 1993).

[36] H. P. Weber, "Comments on the pulse width measurement with two-photon excitation of fluorescence", Phys. Lett. **27A**, 321 (1968).

[37] J. R. Klauder, M. A. Duguay, J. A. Giordmaine, and S. L. Shapiro, "Correlation effects in the display of picosecond pulses by two-photon techniques", Appl. Phys. Lett. **13**, 174 (1968).

[38] S. L. Shapiro and M. A. Duguay, "Observation of subpicosecond components in the mode-locked Nd:glass laser", Phys. Lett. **10**, 698 (1969).

[39] H. A. Pike and M. Hercher, "Basis for picosecond structure in mode-locked laser pulses", J. Appl. Phys. **41**, 4562 (1970).

[40] R. H. Picard and P. Schweitzer, "Theory of intensity-correlation measurements on imperfectly mode-locked lasers", Phys. Rev. A**1**, 1803 (1970).

[41] M. Duguay, J. W. Hansen, and S. L. Shapiro, "Study of the Nd:glass laser radiation", IEEE J. Quantum El. QE-**6**, 725 (1970).

[42] C. K. Hong, Z. Y. Ou, and L. Mandel, "Measurement of subpicosecond time intervals between two photons by interference", Phys. Rev. Lett. **59**, 2044 (1987).

[43] Z. Y. Ou, C. K. Hong, and L. Mandel, "Relation between input and output states for a beam splitter", Opt. Commun. **63**, 118 (1987).

[44] H. Fearn and R. Loudon, "Quantum theory of the lossless beam splitter", Opt. Commun. **64**, 485 (1987).

[45] Z. Y. Ou, "Quantum theory of fourth-order interference", Phys. Rev. A **37**, 1607 (1988).

[46] H. Fearn and R. Loudon, "Theory of two-photon interference", J. Opt. Soc. Am. B**6**, 917 (1989).

[47] Z. Y. Ou and L. Mandel, "Violation of Bell's inequality and classical probability in a two-photon correlation experiment", Phys. Rev. Lett. **61**, 50 (1988).

[48] Z. Y. Ou and L. Mandel, "Observation of spatial quantum beating with separated photodetectors", Phys. Rev. Lett. **61**, 54 (1988).

[49] Z. Y. Ou and L. Mandel, "Further evidence of nonclassical behavior in optical interference", Phys. Rev. Lett. **62**, 2941 (1989).

[50] J. D. Franson, "Bell inequality for position and time", Phys. Rev. Lett. **62**, 2205 (1989).

[51] P. G. Kwiat, W. A. Vareka, C. K. Hong, H. Nathel, and R. Y. Chiao, "Correlated two-photon interference in a dual-beam Michelson interferometer", Phys. Rev. A **41**, 2910 (1990).

[52] Z. Y. Ou, X. Y. Zou, L. J. Wang, and L. Mandel, "Observation of nonlocal interference in separated photon channels", Phys. Rev. Lett. **65**, 321 (1990).

[53] J. D. Franson, "Two-photon interferometry over large distances", Phys. Rev. A **44**, 4552 (1991).

[54] Z. Y. Ou, E. C. Gage, B. E. Magill, and L. Mandel, "Observation of beating between blue and green light", Opt. Commun. **69**, 1 (1988).

[55] Z. Y. Ou, E. C. Gage, B. E. Magill, and L. Mandel, "Fourth-order interference technique for determining the coherence time of a light beam", J. Opt. Soc. Am. B**6**, 100 (1989).

[56] R. Trebino, E. K. Gustafson, and A. E. Siegman, "Fourth-order partial-coherence effects in the formation of integrated-intensity gratings with pulsed light sources", J. Opt. Soc. Am. B**3**, 1295 (1986).

[57] R. Trebino, C. C. Hayden, A. M. Johnson, W. M. Simpson, and A. M. Levine, "Chirp and self-phase modulation in induced-grating autocorrelation measurements of ultrashort pulses", Opt. Lett. **15**, 1079 (1990).

[58] J.-C. M. Diels, J. J. Fontaine, I. C. McMichael, and F. Simoni, "Control and measurement of ultrashort pulse shapes (in amplitude and phase) with femtosecond accuracy", Appl. Opt. **24**, 1270 (1985).

[59] W. Dietel, J. J. Fontaine, and J.-C. Diels, "Intracavity pulse compression with glass: a new method of generating pulses shorter than 60 fsec", Opt. Lett. **8**, 4 (1983).

[60] J. A. Valdmanis, R. L. Fork, and J. P. Gordon, "Generation of optical pulses as short as 27 femtoseconds directly from a laser balancing self-phase modulation, group-velocity dispersion, saturable absorption, and saturable gain", Opt. Lett. **10**, 131 (1985).

[61] T. Matsumoto, M. Baba, T. Kuga, and M. Matsuoka, "Stabilization of a CW mode-locked YAG laser using feedback with an acousto-optic modulator", J. J. A. P. **28**, 391 (1989).

[62] D. E. Spence, P. N. Kean, and W. Sibbett, "60-fsec pulse generation from a self-mode-locked Ti:sapphire laser", Opt. Lett. **16**, 42 (1991).

[63] O. E. Martinez, "3000 Times Grating Compressor with Positive Group Velocity Dispersion: Application to Fiber Compensation in 1.3-1.6 μm Region", IEEE J. Quantum El. QE-**23**, 59 (1987).

[64] T. Matsumoto, L. O. Chua, and M. Komuro, "The double scroll", IEEE Transactions on Circuits and Systems, CAS-**32**, 798 (1985).

[65] P. R. Bevington, *Data Reduction and Error Analysis for the Physical Sciences*, (McGraw-Hill, New York, 1969).